Biophysical Journal
Article

Biophysical Society

H4 Tails Potentially Produce the Diversity in the Orientation of Two Nucleosomes

Hisashi Ishida[1,*] and Hidetoshi Kono[1]
[1]Molecular Modeling and Simulation Group, Department of Quantum Beam Life Science, National Institutes for Quantum and Radiological Science and Technology, Kizugawa, Kyoto, Japan

ABSTRACT Histone tails play an important role in internucleosomal interaction and chromatin compaction. To understand how the H4 tails are involved in the internucleosomal interaction, an adaptively biased molecular dynamics simulation of 63 models of two stacked nucleosomes, each with the H4 tails in different locations, was carried out. This simulation generated a variety of orientations of the separated nucleosomes depending on the formation of the H4 tail bridge between the H4 tails and the DNA of the neighboring nucleosomes. For the models that showed distinctive orientations of the two nucleosomes, the free energies of the separation of the nucleosomes were further investigated using umbrella sampling simulations. The attractive force between the nucleosomes was estimated from the free energies; the force when two H4 tail bridges formed varied from 36 to 63 pN, depending on the formation of the H4 tail-bridge and the interfacial interaction, whereas the force reduced to 15–18 pN after either one of the H4 tail bridges had broken, regardless of the conformation of the H4 tail. Additional simulations of the nucleosomes show that when the H4 tail was truncated, the force between the nucleosomes became repulsive (from −3 to −7 pN). We concluded that the H4 tails potentially produce the diversity in the orientation of the two nucleosomes, which would contribute to the polymorphism of the chromatin structure.

INTRODUCTION

Human genes are encoded by a genome DNA that consists of ∼3,000,000,000 basepairs, and the length of which is ∼2 m long. The genome DNA of eukaryotes, including that of humans, is stored compactly and folded into a higher-order structure called "chromatin". The DNA in chromatin is safely stored in the cell nucleus, which is approximately several micrometers long. At the same time, decompaction of the chromatin structure is also required for the DNA to directly interplay with DNA binding factors such as regulatory proteins and RNA polymerases for transcription, replication, repair, and recombination (1).

The basic structural unit of chromatin is called the "nucleosome", in which ∼150 basepairs of DNA are wrapped around a protein core called a "histone octamer". The histone octamer consists of two H2A-H2B dimers and an $(H3\text{-}H4)_2$ tetramer. Crystal structures show the nucleosome core particle (NCP) has a disk-like shape (2,3). One NCP with 147-bp DNA has a charge of −150 *e* with −294 *e* from the DNA molecule and +144 *e* from the positively charged histone octamer. The electrostatic interaction between negatively charged NCPs can be switched from repulsive to attractive in the presence of ions by their screening the charge of the NCP (4,5).

The N-terminal regions of H2A, H2B, H3, and H4 and the C-terminal region of H2A protrude from the nucleosome structure and are called "histone tails". These histone tails contain many basic Arg and Lys residues and have a large positive charge. These basic residues can be subjected to posttranslational modifications such as acetylation and methylation, which regulate the activity of the genome (1). The positively charged histone tails contribute to the attractive interaction between nucleosomes, which is called "histone tail bridging" (6). Without histone tails, nucleosomes cannot fold into compact conformations due to the DNA-DNA electrostatic repulsion (7,8).

Studies of the arrays of reconstituted NCPs that were linked to each other by linker DNA have revealed detailed interaction between the histone tails and the NCP (6–10). They showed that the positively charged histone tails interact differently with the negatively charged patches of the histone and DNA within the NCP compared with the spatially adjacent NCPs according to the ionic environment, which is mainly categorized into three cases: 1) the intranucleosome interaction, 2) the internucleosome interaction

Submitted March 10, 2017, and accepted for publication July 20, 2017.
*Correspondence: ishida.hisashi@qst.go.jp
Editor: Tamar Schlick.
http://dx.doi.org/10.1016/j.bpj.2017.07.015

within the same NCP array (intraarray), and 3) the internucleosome interaction between different NCP arrays (interarrays). Case 1 is observed in low salt conditions (<0.5 mM Mg^{2+}), and the NCP arrays adopt a fully extended beads-on-a-string 10-nm conformation, where histone tails interact with their own nucleosome. The NCP arrays exhibit a dynamic conformational equilibrium between case 2 and case 3 under physiological ionic conditions (100 mM Na^{+}, >0.5 mM Mg^{2+}) (6). At intermediate ionic concentrations (0.5–2 mM Mg^{2+}, 1 mM Mg^{2+}), the former (the internucleosomal interaction in an intraarray) contributes to folding the NCP array into a secondary chromatin structure (the so-called "30-nm-thick chromatin fibers") (7). At higher (divalent cation) ionic concentrations (>2 mM Mg^{2+}), the internucleosomal interactions in the interarrays aggregate by self-association into large globular oligomers, which stabilize the higher-order tertiary chromatin structure (8). As for the H4 tails, cross-linking experiments showed that the H4 tails of one NCP and the negatively charged region on the surface of the H2A/H2B dimer (called the "acidic patch" (2)) of the neighboring NCP in the intraarray (in case 2) interacted with each other (7,9–11). Moreover, the H4 tails interact with the DNA through either intranucleosomal interaction (in case 1) (10) or internucleosomal interaction between interarrays (in case 3) (10). This indicates that the H4 tails alternatively change interactions with the acidic patch of the histone core and the DNA according to the ionic strength (9,10).

The H4 tails extend in the direction normal to the flat faces of the NCP in the crystal structure, which are located at optimal positions on the surface of the NCP to bridge stacked NCPs (2). The involvement of the H4 tails in the stability of the stacked NCPs has been observed by x-ray and electron microscopy (EM). X-ray (2,3,12), EM (13), and liquid crystalline structures (14,15) have shown that isolated NCP and NCP arrays in vitro form face-to-face stacks with the relatively flat surface of the histone octamer. In crystal structures of the NCP (2,3), two H4 tails from one NCP contact the DNA and the acidic patch of a neighboring NCP, respectively, as crystal packings. The two NCPs are stacked and have the head-to-tail NCP-NCP orientation with their dyad axes reversed. (The head of the NCP is defined as the position of the dyad axis.) In contrast to the head-to-tail orientation of the NCPs, a head-to-head orientation of the NCPs in the stacked structures has been observed by x-ray (12) and EM (13). In the crystal structure of the tetranucleosome, an interaction among α1-helix in H2B (Ser^{38}–Val^{48}), C-terminal αC-helix in H2B (Gly^{104}–Thr^{122}), and α2-helix in H2A (Gly^{46}–Arg^{71}) of neighboring octamers in each dinucleosomal stack was observed (12). The visible N-terminal residues of the H4 tails from residue Val^{21} interact with their own DNA and the DNA on the neighboring NCP within the tetranucleosome unit. In the cryo-EM structure of the histone octamer helical tubes, an interaction between α3-helix in H2B (Ser^{91}–Leu^{101}) and αC-helix in H2B helices of neighboring octamers was observed (13). The visible N-terminal residues of the H4 tails from residue Asn^{25} do not interact with the neighboring histone octamer. Moreover, cryo-EM studies of liquid crystalline structures of isolated NCPs showed that at concentrations from a few millimolar to 150 mM Na^{+} and under pressures of ~2–3 atm, the NCPs stacked on top of each other in a columnar isotropic phase and the NCPs were free to rotate along the axis of the column (14,15). This implies that the H4 tails or the histone octamer in the NCP are not involved in a specific interaction with the neighboring NCPs, so as to fix their rotational movement. However, these static structures cannot explain the large-scale conformational change of the histone tails and nucleosomes.

Computer simulations of the NCPs using coarse-grained (CG) models have been intensively carried out to understand the dynamics of the NCPs (16). A CG model of the NCPs developed by the Takada group uses one particle to represent the amino acids of the histone cores (17) and three particles to represent the nucleotides of the DNA (18). The residue-resolved molecular simulations of trinucleosomes with this CG model showed that the tail acetylation in each histone played an important role in the folding of the trinucleosomes (19). Another CG model of the NCP developed by the Nordenskiöld group (20) uses one particle to represent the amino acids of the histone cores and five particles to represent two basepairs of the DNA. The molecular dynamics (MD) simulations of these models of isolated NCPs with explicit ions showed that the NCPs aggregated in the presence of multivalent ions, where the attractive interactions among the NCPs through histone tails were critical for the aggregation (21). A further CG model for a mesoscale model of chromatin developed by Wedemann and Langowski (22) uses oblate ellipsoids and beads to represent the NCP and the linker DNA, whereas another CG model developed by the Schlick group (23) uses a discrete surface charge optimization model of the NCP with histone tails. The Monte Carlo simulations of the NCP arrays using these CG models showed distinctive characteristics of the NCP array folding depending on the ionic environment and the linker DNA length between nucleosomes (24,25). However, it would be difficult for the CG model to understand the dynamics of the nucleosome in detail at the atomic level. In addition, the CG models still have less reliability for describing the dynamics at a high spatial resolution because it is difficult for their force-field functions to elucidate a significant change in molecular interactions in response to a subtle change in atomic movements.

Several all-atom simulations of stacked nucleosomes were carried out to understand the role of histone tails in the internucleosomal interaction between two NCPs (26–28). Collepardo-Guevara et al. (26) examined the wild-type and acetylated stacked NCP-NCP structural models that were constructed based on the stacked

head-to-head structure of NCP-NCP in the tetranucleosome crystal (12), with one H4 tail placed near the acidic patch of its neighboring nucleosome and the other H4 tail oriented toward the nucleosomal DNA. Zhang et al. (27) investigated the role of the acetylation of Lys^{16} in the H4 tail based on the stacked head-to-tail structure of NCP-NCP in a crystal, where one H4 tail contacts the neighboring acidic patch as crystal packings (3). The all-atom simulations of these structures showed that the acetylated H4 tails weaken the interaction with the acidic patch (26,27). Saurabh et al. (28) considered the stacked NCPs that were constructed so that the NCPs were separated by ~2 nm and aligned in parallel head-to-head orientation. These conventional and steered MD simulations of the modeled structures (with and without tails, at different ionic strengths of 0 and 150 mM salt) showed the separation of the NCP depended on the presence of the tails and the strength of the ionic environment. However, although a steered MD simulation is useful to observe crucial interactions between the NCPs for the stability of the stacked NCPs, the force between the NCPs reached >500 pN when the H4 tail was involved, which is far in excess of the ~5 pN obtained by a single-molecule mechanic measurement (29).

Our motivation is to obtain the free energies of a variety of the internucleosomal interactions between the NCPs, and to understand the role of the histone tails in the internucleosomal interaction from the free energies. As far as we know, systematic analysis of the diversity of the internucleosomal interactions has not been reported at the atomic level. Previously, we investigated the intranucleosomal interaction: the dynamics of DNA breathing and unwrapping from the histone octamer surface in the mononucleosome (30–32). This work about internucleosomal interaction will give further insight into the understanding of the polymorphic nature of the chromatin structure. To obtain a variety of conformations of the separated NCPs, we carried out an adaptively biased MD (ABMD) simulation of the stacked NCPs. We further carried out umbrella sampling simulations to obtain the free energies of the models that had distinctive orientations in the ABMD simulation. We found that the H4 tails played an important role in the diversity of the orientation of the separated NCPs. In this article, we report 1) the diversity of the NCP-NCP conformations that were determined by how the H4 tail-bridge formed, and 2) the free energies of the separated NCPs.

MATERIALS AND METHODS

Modeling of two nucleosomes

To prepare the initial atomic structure of the two nucleosomes, the positions and orientations of two stacked nucleosomes in the x-ray structure of the *Escherichia coli* tetra-nucleosome with a 167-bp NRL (PDB: 1ZBB, resolution 2.20 Å) (12) were used. The missing parts of the histone tails in the structure were modeled by using the corresponding parts in the *Thermus aquaticus* mononucleosome (from PDB: 1KX5, resolution: 1.9 Å) (3) as templates.

We refer to the DNA, H4 tail, and histone (excluding the H4 tail) of one NCP as DNA_1, H4 $tail_1$, and $histone_1$, and those of the other NCP as DNA_2, H4 $tail_2$, and $histone_2$ (see Fig. 1). $DNA_{1/2}$ have 167 basepairs. (The sequence of the nucleotides in the $DNA_{1/2}$ is listed in Table S1.) Note that even though a nucleosome with ~147-bp DNA is usually referred to as the "NCP", in this study, so long as there is no confusion, we also refer to the nucleosome with 167-bp $DNA_{1/2}$ as the "NCP". To reduce the size of the system, the N-terminal residues of H3 (residues Ala^1 to Pro^{30}) and H2B (residues Pro^2 to Lys^{21}) that protruded from the DNA gyres were truncated. In the initial structure, His^{18} of the H4 $tail_{1/2}$ is located between $DNA_{1/2}$ gyres. The distance between the phosphorus atom of Cyt^{22}/Cyt^{189} in $DNA_{2/1}$ (which is closest to His^{18} of the H4 $tail_{1/2}$) and the phosphorus atom of Thy^{229}/Thy^{62} in $DNA_{1/2}$ (which is closest to Cyt^{22}/Cyt^{189} in $DNA_{2/1}$) was used as the indicator for the orientation of the NCPs, and is referred to as "$d(DNAs)_{1/2}$". $d(DNAs)_{1/2}$ were monitored to observe how the NCP-NCP conformation changed during the separation of the NCPs. In this study, d (the distance between the centers of mass of rigid parts of each NCP, Gly^{33}–Ala^{135} of H3, Asn^{25}–Gly^{102} of H4, Lys^{15}–Thr^{120} of H2A, and Pro^{50}–Lys^{125} of H2B histones) was set as the reaction coordinate for our simulations (see "ABMD Simulation"). The values of d and $d(DNAs)_{1/2}$ in the initial structure were 57.2 and 9.4/9.3 Å, respectively. In this study, we call the orientation of the separated NCPs in which $d(DNAs)_1 > d(DNAs)_2$, $d(DNAs)_1 < d(DNAs)_2$, and $d(DNAs)_1 \sim d(DNAs)_2$ "RIGHT", "LEFT", and "PARALLEL", respectively. Moreover, to understand how each of the H4 tails (residues Ser^1–Ile^{26}) interacts with the DNA of the neighboring NCP, their atomic interactions within a distance of 3.5 Å were monitored. The H4 $tail_{1/2}$-bridge was defined as being formed at d when atomic interactions between any residue from Ser^1 to Ile^{26} of the H4 $tail_{1/2}$ and the $DNA_{2/1}$ were observed in >10% of all the trajectories at d.

Simulated annealing in vacuum

All the MD simulations were carried out using an MD simulation program called SCUBA (33–37) with the AMBER *ff*99SB (38), *ff*99bsc0 (39), and *ff*99ions08 (40) force fields for histones, DNAs, and ions, respectively. To optimize the conformation of the modeled tails, simulated annealing (SA) was performed in vacuum by assuming a distance-dependent dielectric constant of $4.0r$ with the value of r in Ångstroms. After the SA was repeated

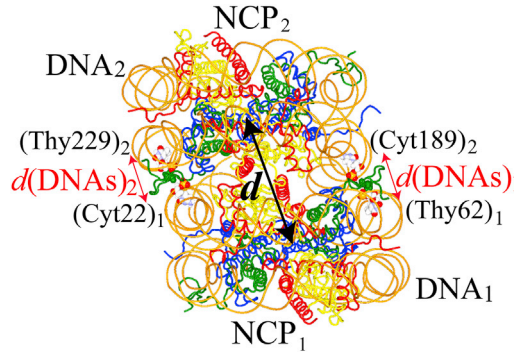

FIGURE 1 The initial structure of the two nucleosomes. Two NCPs are shown in the tube model. Cyt^{22} and Thy^{62} in DNA_1 and Cyt^{189} and Thy^{229} in DNA_2 are shown in the CPK model. His^{18} of the H4 tail in the $NCP_{1/2}$ is shown in the CPK model in green. H3, H4, H2A, and H2B are shown in blue, green, yellow, and red, respectively. The N-terminal residues of H3 (Ala^1 to Pro^{30}) and H2B (Pro^2 to Lys^{21}) that protruded from DNA gyres were truncated. The reaction coordinate, d, and between the phosphorus atom of Cyt^{22}/Cyt^{189} in $DNA_{1/2}$ and the phosphorus atom of Thy^{229}/Thy^{62} in $DNA_{2/1}$, $d(DNAs)_{1/2}$, at the initial structure were 57.2 Å and 9.4/9.3 Å, respectively. To see this figure in color, go online.

150 times, the 63 lowest-energy structures were selected as representatives of the two NCPs with H4 tails located in different positions. Details are given in the Supporting Material.

MD simulations of the systems in water

After the SA, the 63 structures were each placed in an aqueous medium. Each system of the two NCPs was placed in a rectangular box ~140 × 165 × 215 Å with the axis of the stacking of the two NCPs in the z direction. In each box, all atoms of the two NCPs were separated >15 Å from the lateral edge of the box and 40 Å from the top edge of the box. To neutralize the charges of each system, sodium ions were placed at positions with large negative electrostatic potential. Moreover, sodium and chloride ions were added to each box at random positions at a concentration of 150 mM NaCl. Then ~135,000 TIP3P water molecules (41) were added to surround each system. In total, each system comprised ~460,000 atoms.

All the systems were equilibrated at a constant pressure of one bar and a temperature of 300 K for 5 ns. The dielectric constant used was 1.0 and the van der Waals interactions were evaluated with a cutoff radius of 9 Å. The particle-particle particle-mesh method (42,43) was used for the electrostatic interactions for the direct space cutoff of 9 Å. The Langevin dynamics algorithm was utilized to control the temperature and pressure of the system. The coupling times for the temperature and pressure control were both set at 2 ps^{-1}. The SHAKE algorithm (44,45) was used to constrain all the bond lengths involving hydrogen atoms. The leap-frog algorithm with a time step of 2 fs was used throughout the simulation to integrate the equations of motion. Details are given in the Supporting Material.

ABMD simulation

To observe the separation of the NCPs in the two NCPs, the ABMD method (46) combined with the multiple walker method (47) was employed in SCUBA. The equations of motion used in the ABMD method are expressed as (46)

$$\begin{aligned} m_a\frac{d^2\mathbf{r}_a}{dt^2} &= \mathbf{F}_a - \frac{\partial}{\partial \mathbf{r}_a}U[t\,|\,\sigma(\mathbf{R})], \\ \frac{\partial U(t\,|\,d)}{\partial t} &= \frac{k_\mathrm{B}T}{\tau_F}K[d-\sigma(\mathbf{R})], \end{aligned} \tag{1}$$

where $\mathbf{R} \equiv (\mathbf{r}_1, \ldots, \mathbf{r}_N)$ are the coordinates of the NCP, and N is the number of atoms in the two NCPs. d is the reaction coordinate, and $\sigma(\mathbf{R})$ is a function to give the value of the reaction coordinate. k_B is the Boltzmann constant, T is the constant temperature, τ_F is the flooding timescale, and K is the kernel that has distribution around the reaction coordinate. The first equation is for atom a, with an additional force coming from the biasing potential $U(t|d)$ with an ordinary atomic force of $\boldsymbol{F}_a$. The second equation is the time-evolving equation of the biasing potential. Details of the ABMD algorithm used in SCUBA are given in (36).

The ABMD simulations were carried out at a constant volume and a temperature of 300 K for 134 ns per system (a total of 8.4 μs for all 63 systems). The value of the reaction coordinate in the initial structure was 57.2 Å, and the range of the reaction coordinate for the ABMD simulations was set at $d \geq$ 50.0 Å. The resolution of the reaction coordinate, Δd, was set at 1.0 Å. The relaxation time for the free-energy profile in Eq. 1, τ, was set at 5000 ps. The two NCPs separated from each other in many systems, as shown in Fig. 2. The conformation of the NCPs was stored every 1 ps for analysis.

Umbrella sampling simulations

Theoretically, for large enough τ_F and small enough width of the kernel, $U(t|d)$ converges toward the free-energy $F(d)$ times −1 as the simulation time elapses from $t = 0$ to ∞ (46). Using τ_F with a certain finite amount of time, the biasing potential (free-energy landscape times −1) fluctuates around the free energy during the ABMD simulation (36,46). However, the biased potential did not show any fluctuation as shown in Fig. S1 *a*, indicating that the convergence of the free energy is not accomplished. Moreover, as 63 systems moved to different conformations from each other as shown in Fig. 3, the identical biasing potential in our ABMD simulation would not be appropriate to represent possible different free energies for each system. In this study, we paid attention to some models that we observed had distinctive orientations of the NCPs in the ABMD simulation (LEFTs 1–3, RIGHTs 1–3, and PARALLELs 1–2 as shown in Fig. 3). Instead of continuing the ABMD simulation, we carried out umbrella sampling simulations of these models to obtain their free energies.

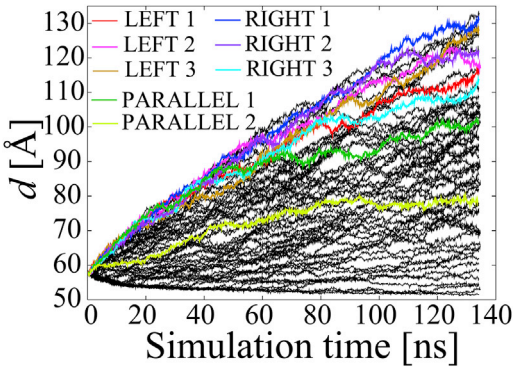

FIGURE 2 The evolution of the reaction coordinate, d, of all 63 models during the ABMD simulation. The eight models that were selected to evaluate the free energies using umbrella sampling simulations are colored (*red*, *magenta*, and *brown* in LEFTs 1–3; *blue*, *cyan*, and *purple* in RIGHTs 1–3; and *dark green* and *light green* in PARALLEL 1–2, respectively). To see this figure in color, go online.

The weighted histogram analysis method (48) was used to evaluate the free energy from the sampled trajectories in the umbrella sampling simulations. In the weighted histogram analysis approach, the unbiased probability distribution $P(\mathbf{R})$ is calculated from the biased probability distribution of the sampled coordinates as

$$\begin{aligned} P(\mathbf{R}) &= \sum_{i=1}^{N_\mathrm{win}} n_i\,(\mathbf{R})P_i^{(b)}(\mathbf{R}) \\ &\quad\times\left(\sum_{j=1}^{N_\mathrm{win}} n_j\,(\mathbf{R})\exp\left\{\left[F_j - V_j(\mathbf{R})\right]/k_\mathrm{B}T\right\}\right)^{-1}, \end{aligned} \tag{2}$$

where $\mathbf{R}$ is the atomic coordinates, N_win is the number of windows, $n_i(\mathbf{R})$ is the number of data points in the ith window, $P_i^{(b)}(\mathbf{R})$ is a biased probability from the raw data obtained in the umbrella sampling simulation, and $V_j(\mathbf{R})$ is the biasing potential in the jth window. In this study, $V_j(\mathbf{R})$ was selected to be the sum of a harmonic potential and the ABMD biasing potential in the final stage of the ABMD simulation, which has the form

$$\begin{aligned} V_i(\mathbf{R}) &= k_i\left[d(\mathbf{R}) - d_i^\mathrm{fix}\right]^2 + c\bullet\{U_\mathrm{abmd}[d(\mathbf{R})] \\ &\quad - U_\mathrm{abmd}(d_0)\}, \end{aligned} \tag{3}$$

where $d(\mathbf{R})$ is the umbrella sampling coordinate, which was set to be $\sigma(\mathbf{R})$. d_i^fix is a fixed distance to sample umbrella coordinates of $d(\mathbf{R})$ around the desired position of d_i^fix. The initial coordinates of $\mathbf{R}$ for the ith window

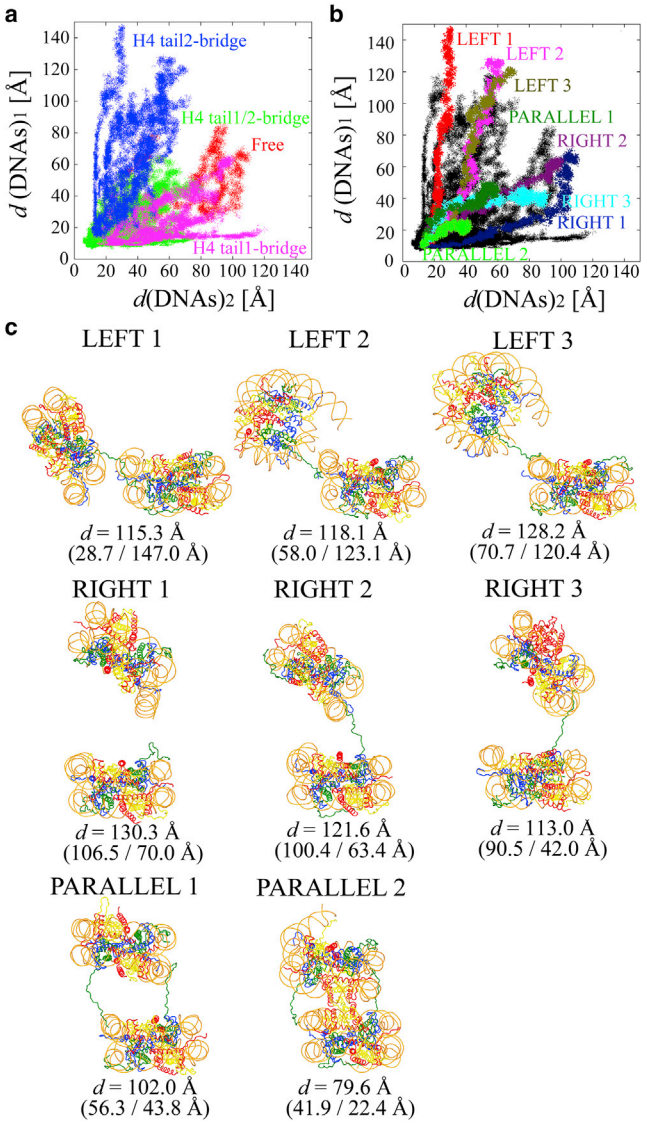

FIGURE 3 (*a*) The trajectories of $d(\mathrm{DNAs})_{1/2}$ of all 63 models during the ABMD simulation. The points are colored in red, blue, and purple when only one H4 tail_1-bridge formed, when only one H4 tail_2-bridge formed, and when both H4 $\mathrm{tail}_{1/2}$-bridges formed, respectively. (*b*) The trajectories of $d(\mathrm{DNAs})_{2/1}$ in LEFTs 1–3, RIGHTs 1–3, and PARALLELs 1–2. The colors are the same as in Fig. 2. (*c*) The final structures in LEFTs 1–3, RIGHTs 1–3, and PARALLELs 1–2 with d and $d(\mathrm{DNAs})_{2/1}$. To see this figure in color, go online.

were selected from the trajectories that had similar d_i^{fix} in the ABMD simulation. The values of d_i^{fix} were set from 58 Å to 110, 115, and 110 Å for LEFTs 1–3; 122, 118, and 105 Å for RIGHTs 1–3; and 100 and 80 Å for PARALLELs 1–2, respectively, with intervals of 1 Å ($i = 1,\ldots, N_{\mathrm{win}}$). k_i is an arbitrary harmonic force constant, which was set at 0.2 kcal/mol/Å^2. U_{abmd} is the biasing potential at the final stage of the ABMD simulation (Fig. S1 *a*). Here, d_0 is a constant such that $U_{\mathrm{abmd}}[d(\mathbf{R})] - U_{\mathrm{abmd}}(d_0)$ is zero at $d = d_0$. c is the arbitrary constant to scale U_{abmd}. In this study, $c = 0.25$ and 0.0 were used for $d > d_0$ and $d \le d_0$ with $d_0 = 60.0$ Å, respectively (see Fig. S1 *b*). The umbrella sampling simulation was carried out for 30 ns. The conformations of the NCPs were stored every 1 ps for analysis. The trajectory for the last 20 ns was used for the calculation of the free-energy landscape.

The relative free-energy $F(\mathbf{R})$ at a given $\mathbf{R}$ is obtained as

$$F(\mathbf{R}) = -k_{\mathrm{B}}T \ln P(\mathbf{R}). \tag{4}$$

Details are given in the Supporting Material.

Umbrella sampling simulations of the two NCPs without the H4 tails

To understand the role of the H4 tails, umbrella sampling simulations of the two NCPs without the H4 tails were also carried out for LEFT 1, RIGHT 1, and PARALLEL 1, which had distinctive orientations of the NCPs. Details are given in the Supporting Material.

The conformational entropies of the H4 and H2A tails

The conformational entropies of the H4 and H2A tails were calculated using the quasiharmonic approximation (49) as follows:

$$S_{\mathrm{conf}} = 0.5\, k_{\mathrm{B}} \ln \det\left[\mathbf{1} + \left(k_{\mathrm{B}}Te^2/\hbar^2\right)\boldsymbol{\sigma}\right], \tag{5}$$

where e is *Euler*'s number, and $\hbar$ is Planck's constant divided by 2π. $\boldsymbol{\sigma} = \langle \boldsymbol{x}\, \boldsymbol{x}^T \rangle$ represents the mass-weighted covariance matrix, where $\boldsymbol{x}$ is the coordinates of the H4 $\mathrm{tail}_{1/2}$ (residues 1–26) and the H2A $\mathrm{tail}_{1/2}$ (residues 1–17). Details are given in the Supporting Material.

Computational time

All the simulations, requiring a total time of 27 μs (8.4 μs for the ABMD simulation and 18.6 μs for the umbrella sampling simulations), were mainly performed on the Fujitsu BX900 and SGI ICE X supercomputers at Japan Atomic Energy Agency. The total computational time was >30,000,000 CPU core hours.

RESULTS

The diversity in the orientation of the two separated NCPs

The time evolution of d and the trajectory of $d(\mathrm{DNAs})_{2/1}$ for all 63 models during the ABMD simulation show that a variety of types of separation of the NCPs occurred in LEFTs, RIGHTs, and PARALLELs (Figs. 2, 3, and S2). As only the H4 tail conformation was different in the initial 63 configurations, the origin of the diversity in the separation must have come from the H4 tails. To understand what kind of interactions between the H4 tails and NCPs correlated with the diversity of separation, the formation of the H4 tail-bridge between H4 $\mathrm{tail}_{1/2}$ and $\mathrm{DNA}_{2/1}$ was analyzed. Fig. 3 *a* shows that the orientations of the NCPs in LEFTs, RIGHTs, and PARALLELs were different from each other, where one H4 tail-bridge between H4 tail_1 and DNA_2, one H4 tail-bridge between H4 tail_2 and DNA_1, and two H4 tail-bridges between H4 $\mathrm{tail}_{1/2}$ and $\mathrm{DNA}_{2/1}$ formed, respectively. These results clearly show that the diversity of separation of the NCPs is correlated with the formation of the H4 tail-bridge interaction.

The free energies of the two separated NCPs

We selected eight out of 63 models that had distinguishing internucleosomal interactions (LEFTs 1–3, RIGHTs 1–3, and PARALLELs 1–2 (Fig. 3)), and calculated their free energies using umbrella sampling simulations. Fig. 4 shows all the free energies of the NCPs against d. (The root mean square errors in the free energies were estimated to be ~0.3 kcal/mol against d (Fig. S3).) The free energies increased from 0 at $d = 58$ Å up to ~20 kcal/mol at each final position of $d = \sim 80-120$ Å. This indicates that the internucleosomal interaction between the NCPs was attractive. It should be noted that in the LEFTs 1–3 the distance between one NCP and the image of the periodically neighboring NCP in the direction of z was <15 Å at $d \geq 106$, 107, and 107 Å, respectively (see Fig. S4), indicating that the free energy in LEFTs 1–3 at $d > 105$ Å may include an artifact from the periodic boundary condition.

To understand how the H4 tail-bridge interaction correlated with the orientation of the NCPs, the population of the interaction between each residue in the H4 tail and the DNA was counted as shown in Figs. 5 and S5. (As a reference, the number of atomic contacts between the NCPs is shown in Fig. S6.) Figs. 5 and S5 show that a high population around $Arg^{19}-Arg^{23}$ was observed in all the cases in the range of $d = \sim 58$ to 70 Å. On the contrary, the population around $Ser^{1}-Lys^{16}$ varied among the cases. In LEFTs 1–3, H4 $tail_1$ maintained the bridge interaction, during which $d(DNAs)_2$ gradually increased but did not reach >30, 60, and 60 Å, respectively (see Figs. 6 and S7). This indicates that the strong interaction between H4 $tail_1$ and DNA_2 prevented $d(DNAs)_2$ from increasing during the separation of the NCPs. On the other hand, after H4 $tail_2$ detached from DNA_1 at $d = 75$, 74, and 81 Å in LEFTs 1–3, respectively, $d(DNAs)_1$ rapidly increased. Consequently, the maintenance of the H4 $tail_1$-bridge and the breakage of the H4 $tail_2$-bridge facilitated the opening of the NCPs on the left side.

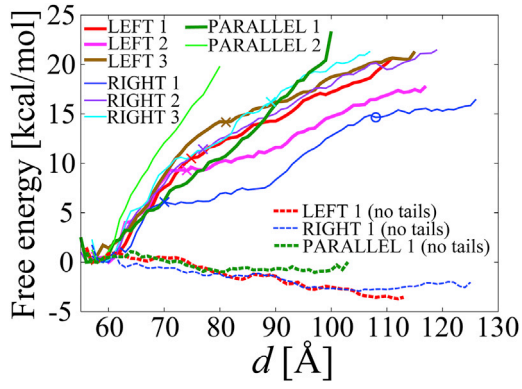

FIGURE 4 The free energies of the two separated NCPs against d in LEFTs 1–3, RIGHTs 1–3, and PARALLELs 1–2. The unit is Å. The colors are the same as in Fig. 2. To see this figure in color, go online.

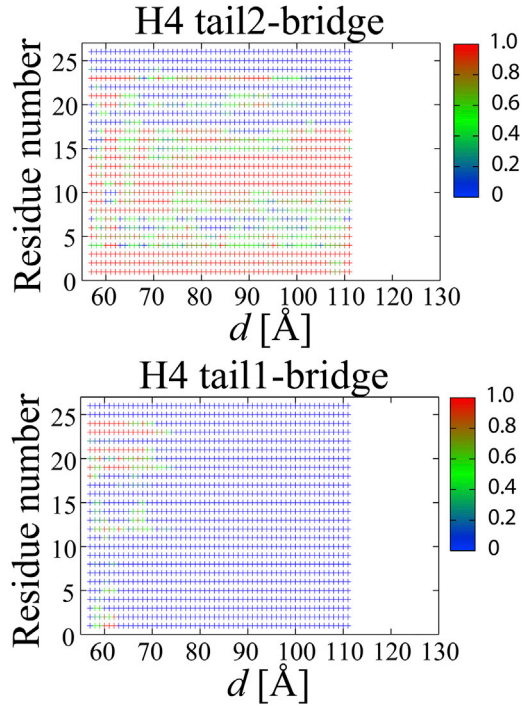

FIGURE 5 The average population of residues that participated in the formation of H4 $tail_{1/2}$-bridge in LEFT 1. The average was calculated according to Eq. S8. The average population in LEFTs 2–3, RIGHTs 1–3, and PARALLELs 1–2 are shown with LEFT 1 in Fig. S5. To see this figure in color, go online.

In RIGHT 1, after H4 $tail_2$ detached from DNA_1 at $d =$ 70 Å (see a *cross* on the *blue curve* in Fig. 4), the H4 $tail_1$-bridge gradually stretched until H4 $tail_1$ detached from DNA_2 at $d = 108$ Å (see *open circle*). The increase in the free energy substantially stopped after $d = \sim 108$ Å because the attraction between the NCPs by H4 $tail_{1/2}$-bridges disappeared. Fig. S7 *b1* shows that from $d = 108$ to 123 Å, $d(DNAs)_1$ changed from 36.8 to 54.8 Å whereas

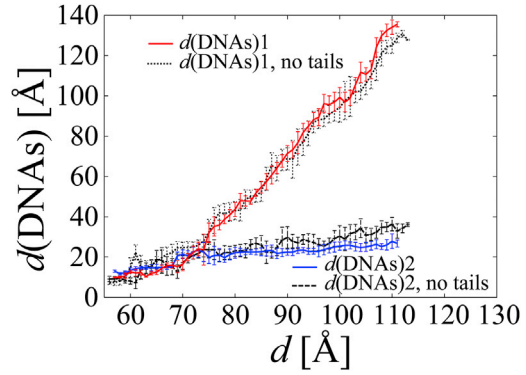

FIGURE 6 $d(DNAs)_{2/1}$ against d in LEFT 1 with and without the H4 tails. The average and RMSD were calculated according to Eqs. S8 and S9, respectively. $d(DNAs)_{2/1}$ in LEFTs 2–3, RIGHTs 1–3, and PARALLELs 1–2 are shown with LEFT 1 in Fig. S7. To see this figure in color, go online.

$d(\mathrm{DNAs})_2$ changed from 99.2 to 108.6 Å, showing that the change of $d(\mathrm{DNAs})_1$, 18.0 Å, was larger than that of $d(\mathrm{DNAs})_2$, 9.4 Å. This indicates that the electrostatic repulsion between DNAs at $d(\mathrm{DNAs})_1$ was stronger than the repulsion at $d(\mathrm{DNAs})_2$, resulting in the partial recovery of a parallel conformation from the tilted conformation (see also Fig. S8 *b1*). The recovery from the tilted conformation toward a parallel conformation after the two H4 $\mathrm{tail}_{1/2}$-bridges were broken was also observed in two models in the ABMD simulation, as shown in Fig. S2 *d*. In RIGHTs 2 and 3, the H4 tail_1 maintained the bridge interaction in a similar way to RIGHT 1, whereas H4 tail_2 detached from DNA_1 at $d = 77$ and 89 Å. When $d(\mathrm{DNAs})_2$ increased to reach ~100 Å in RIGHTs 2 and 3, the separation of the NCPs reached $d = 120$ and 110 Å, respectively, as shown in Fig. S7, *b2* and *b3* (see also Fig. S8, *b3* and *b4*).

In PARALLELs 1 and 2, both H4 $\mathrm{tail}_{1/2}$-bridges were retained. The sharp rise of the free energies up to ~20 kcal/mol at $d = 80-100$ Å was thought to be because the two H4 $\mathrm{tail}_{1/2}$-bridges strongly prevented the NCPs from separating from each other. In PARALLEL 1, although the H4 tail_2-bridge around $\mathrm{Arg}^{19}-\mathrm{Arg}^{23}$ disappeared at $d =$ 74 Å, $\mathrm{Ser}^1-\mathrm{Lys}^5$ of the H4 tail_2 newly participated in the H4 tail_2-bridge formation after $d = 74$ Å (Fig. S5 *c1*), which maintained the parallel conformation. In PARALLEL 2, in addition to the two H4 $\mathrm{tail}_{1/2}$-bridges, internucleosomal interactions among the N-terminal of histone $\mathrm{H2A}_{1/2}$, the C-terminal of histone $\mathrm{H2B}_{1/2}$, and $\mathrm{DNA}_{2/1}$ were intermittently retained (data not shown). Moreover, Lys^{117} in the C-terminal αC-helix of histone $\mathrm{H2B}_1$ had a new interaction with Pro^{47} in a loop between α1-helix and β1-sheet of $\mathrm{H2B}_2$ at $d =$ ~80 Å, which did not exist in the initial structure (Fig. S8 *c3*). These internucleosomal interactions among $\mathrm{H2A}_{1/2}$, $\mathrm{H2B}_{1/2}$, and $\mathrm{DNA}_{2/1}$ are thought to be electrostatically stabilized and have contributed to the rapid rise in the free energy to 20 kcal/mol, whereas the two NCPs were still relatively close to each other ($d = 80$ Å).

Figs. 5 and S5, *a* and *b*, show that H4 tail_1 in LEFTs 1–3 and H4 tail_2 in RIGHTs 1–3 detached from DNA_2 and DNA_1 at $d = 75$, 74, 81 Å and $d = 70$, 77, 89 Å, respectively (see also Fig. S8, *a* and *b*). These values of d (the *crosses* in Fig. 4) roughly correspond to the values of d when the increase in their free energies slowed down. This indicates that the maintenance of the two H4 $\mathrm{tail}_{1/2}$-bridges greatly contributed to the free energy until one H4 tail-bridge broke. After that, the free energy gradually increased until the remaining bridge was broken.

The H4 tail-bridge interaction is the main contributor to the free energy

To confirm whether the H4 tails were the main contributor to the free energies, the free energies of the NCPs without the H4 tails for LEFT 1, RIGHT 1, and PARALLEL 1 were calculated as shown in Fig. 4. The free energies of the NCPs without the H4 tails had broad peaks of ~1−2 kcal/mol at $d =$ ~58−75, ~58−63, and ~58−70 Å in LEFT 1, RIGHT 1, and PARALLEL 1, respectively. Fig. S6 *d* shows that the composition of the interfacial interaction (between $\mathrm{histone}_1$ and $\mathrm{histone}_2$; $\mathrm{histone}_{1/2}$ and $\mathrm{DNA}_{2/1}$; and DNA_1 and DNA_2) varies among the three cases. These peaks of ~1−2 kcal/mol seem to come from interfacial interaction between the stacked NCPs. After the interfacial interaction disappeared, the free energies became negative, indicating that the interaction between NCPs without the H4 tails became repulsive. This is consistent with experimental data, which shows that the removal of the H4 tails prevents the NCP array from folding (7) and oligomerizing (8). The comparison of the NCP–NCP conformations with and without the H4 tails at the same d indicates that without the H4 tails, $d(\mathrm{DNAs})_2$ increased by 4.2 Å on average in the range of $d =$ ~75 to 111 Å for LEFT 1, and $d(\mathrm{DNAs})_1$ increased by 4.0 Å on average in the range of $d =$ ~63 to 107 Å for RIGHT 1 (Figs. 6 and S7, *a* and *b*). This indicates that the DNA–DNA repulsion was strong between the NCPs because they lost the attractive interaction that is produced by H4 tails. Consequently, we confirmed that the H4 tail-bridge was the main contributor to the attractive interaction between the NCPs in the simulations.

The H4 tail-bridge enthalpically stabilizes the stacked NCPs

The screening of the electrostatic repulsive interaction between negatively charged NCPs has been suggested to be due not only to the presence of a cation such as a sodium ion and a magnesium ion (4,28) but also the flexible cationic tails that form bridges and reduce the repulsion between NCPs (28,50). We analyzed the screening of the negatively charged NCPs by the positively charged Lys and Arg in the H4 and H2A tails. Fig. S9 shows that the H4 tails mainly interacted with the atoms of the phosphate groups in the DNA (in PARALLEL1). This indicates that the H4 tail-bridge screens the DNA-DNA repulsion between the NCPs to stabilize the stacked NCPs. Fig. S9 also shows that the H4 tail-bridge was dynamic as the sites of their interactions continuously changed during the simulation. The major interaction between the H4 tails and the phosphate groups, and the dynamic behavior of the H4 tails, were also observed in the other cases, LEFTs 1–3, RIGHTs 1–3 (figure not shown), and PARALLEL 2 (Figs. S9 *d–f*). As for the H2A tails, they interacted with the DNA of the neighboring NCP at $d = 58$ Å in PARALLEL 1 (Fig. S9 *a*) but not at $d >$ 62 Å, which was similar to other cases except in PARALLEL2, where the H2A tail-bridge was observed at $d = 80$ Å (Fig. S9 *f*). This may indicate that the H2A tail stabilizes the stacking of the NCPs when they are close together.

The secondary structure of the H4 and H2A tails was also analyzed as shown in Fig. S10. The structures observed at

all d were mainly turn or coil. The regular secondary structures such as α-helix, 3_{10}-helix, and β-strand were not substantially observed at any d. This trend was true for other cases (LEFTs 1–3, RIGHTs 1–3, and PARALLEL 2) (see Table S2). These results indicate that the H4 tails were disordered at any d, thus the stretching of the H4 tail itself (the internal energy within the H4 tail) as d increased would not significantly contribute to the free energy.

Moreover, the conformational entropies of the H4 and H2A tails were analyzed using the quasiharmonic approximation (49). Overall, the conformational entropies of the H4 tails increased as d decreased whereas those of the H2A tails were constant (Fig. S11). These observations indicate that the enthalpically unfavorable breakage of the H4 tail-bridge counteracted the entropically favorable increase in the flexibility of the tails during the separation of the NCPs. Consequently, strong electrostatic interaction for screening is thought to be an important enthalpic component for the stabilization of the nucleosome stacking, and the increase in the free energy is thought to be mainly from the breakage of the electrostatic interaction.

Forces for the two separated NCPs

The magnitude of the attractive force between the NCPs was calculated from the slope of the free energies before and after one H4 tail-bridge broke. The force between NCP_1 and NCP_2, which was derived from the interfacial interaction and the two H4-tail bridges, was estimated from the regression line for the free energy in the range of d = 58 Å to d just before the first H4 tail-bridge had broken (shown by *crosses* in Fig. 4). This resulted in 48.0, 49.3, 47.4, 41.2, 47.4, and 36.6 pN in LEFTs 1–3 and RIGHTs 1–3, respectively (6.97 pN = 1 kcal/mol/nm). The force between NCP_1 and NCP_2, which is derived from the remaining bridge, was estimated from the regression line for the free energy in the range of d at the first bridge breakage to the final d to be 18.2, 15.6, 14.9, 18.4, 16.8, and 18.4 pN in LEFTs 1–3 and RIGHTs 1–3, respectively. Note that in LEFTs 1 and 3, the free energy at d = 111 and 115 Å, respectively, was not used in the analysis because the free energy was not reliable. In fact, the number of data points at d = 111 and 115 Å ($n_i(d)$ in Eq. 2) to calculate the free energy was <1% of the number of data points (20,000) for each window. In RIGHT 1, d = 107 Å, just before all the H4 $tail_{1/2}$-bridges broke, was used as the final d. The attractive force between NCP_1 and NCP_2 due to the two H4 $tail_{1/2}$-bridges in PARALLEL 1 was estimated to be 35.6 pN using the values of the free energy in the range of d = 58 to 99 Å (as the free energy at d =100 Å was not reliable for the aforementioned reason), which is roughly double of ∼15−18 pN from one tail bridging. Similarly, using the values of the free energy in the range of d = 58 to 80 Å, the force in PARALLEL 2 was estimated to be 62.6 pN, indicating that the strong internucleosomal interactions among the N-terminal of the $H2A_{1/2}$, C-terminal $H2B_{1/2}$, and $DNA_{2/1}$ (Figs. S6 *c2* and S8 *c3*) contributed to the large force. The force between NCP_1 and NCP_2 without the H4 tails was estimated using the regression line for the free energy in the range of d = 70, 62, and 65 to 100 Å in LEFT 1, RIGHT1, and PARALLEL1, respectively. The free energy at d > 100 Å was not used, as the increase in the free energy may include an artifact from the periodic boundary condition (see Fig. S4). This resulted in −7.2, −4.3, and −2.7 pN for LEFT 1, RIGHT 1, and PARALLEL 1, respectively.

DISCUSSION

Comparison of the computational results from the NCPs with the experimental data

The free energies of the two separated NCPs can give an insight into the understanding of the internucleosomal interaction between NCPs observed in experiments. The free energies in LEFTs 1–3, RIGHTs 1–3, and PARALLELs 1–2 were stable at d = ∼58 Å. The results of the all-atom simulation of the stacked NCPs with all the tails and 147 × 2 bp DNAs at 150 mM NaCl by Saurabh et al. (28) showed that the inter-NCP distance fluctuated between ∼56 and 58 Å, which is consistent with our result. It should be noted that the NCP-NCP orientation was different from that in our study; the NCPs in their system were in a head-to-head orientation with their dyad axes aligned parallel to each other (the dyad-dyad angle of the NCPs was 0°). In contrast, the dyad-dyad angle of the NCPs at d = ∼58 Å in our system was >20° (12). These results indicate that the stability of the NCPs may not depend on the rotation of the NCP. This independence is consistent with the experimental data that the stacked NCPs in the columnar isotropic phase of liquid crystalline structures were free to rotate along the axis of the column (14,15).

We found that the free-energy curves against d were different among LEFTs 1–3, RIGHTs 1–3, and PARALLELs 1–2. This is thought to come from the difference in the direct interfacial interaction between the histones (excluding the H4 tails) (Fig. S6) and the difference in the H4 tail-bridge interaction (Figs. 5 and S5). The former is estimated to be 1−2 kcal/mol from the results of the free energies of the NCPs without the H4 tails (Fig. 4). The latter is evaluated by how far H4 tail-bridges were retained. Arg^{19}−Arg^{23} at the root of the H4 $tails_{1/2}$ were located at the interface between NCP_1 and NCP_2, and interacted with $DNA_{2/1}$ at d = ∼58−70 Å. Arg^{19}−Arg^{23} appear to contribute to the large increase in the free energy at d = ∼58−70 Å, before the stabilized interfacial interaction is broken. At d > ∼70 Å, some of Ser^{1}−Lys^{16} were involved in forming the H4 $tail_{1/2}$-bridges. In LEFTs 1–3 and RIGHTs 1–3, the d values

when the first H4 tail-bridge broke are shown by crosses in Fig. 4. The farther the H4 $tail_{1/2}$-bridges were retained, the more the free energy increased. The wide range of d values (75, 74, 81, 70, 77, and 89 Å) at which the bridge was broken may explain the large variation in the force-extension curve of the NCP arrays in a single-molecule experiment (51). In this experiment (51), a single-molecule force spectroscopy on folded NCP arrays (10 chromatin fibers reconstituted on 15 repeats of a 197-bp nucleosome) at the physiological salt concentration of 100 mM K^+ and 2mM Mg^{2+} showed that the transitions from a folded NCP array to a string of nucleosomes in an extended conformation occurred at different extensions for 10 different fibers (51). The large variation in extension was attributed to the variation in the composition of the NCP array (such as an incomplete NCP-array reconstitution and/or partial dissociation of nucleosomes) (51). The variation in the H4 $tail_{1/2}$-bridges observed in our study may also contribute to the variation in extension.

The internucleosomal stretching force was estimated to be 4.5 pN by a single-molecule mechanic measurement of the 197-bp NRL nucleosomal array of 25 nucleosomes with 50-bp linker DNA at the physiological salt concentration of 100 mM K^+ and 2 mM Mg^{2+} (29). The force was considered to come from an extension of a single stack of perpendicular nucleosomes (29). The height of the nucleosomal array of 25 stacked NCPs was measured to be ~200 nm, meaning that the length of stacking per one NCP was ~80 Å. This indicates that these NCPs can have irregular stacking conformations as observed in our study at $d = \sim 80$ Å where the neighboring NCPs usually interacted with each other by one H4 tail-bridge. As cross-linking experiments have suggested that the internucleosomal interaction in the intraarray was between the H4 tails and the acidic patch of the neighboring NCP (7,9,10), the internucleosomal stretching in the single molecule experiment may be derived from the H4 tail–acidic patch interaction.

The results of the all-atom steered MD simulation of two NCPs by Saurabh et al. (28) indicate that the H4 tail-acidic patch interaction significantly reduced at $d = \sim 80$ Å because the Arg^{23}-acidic patch interaction that was observed at $d = \sim 58-60$ Å was not maintained up to $d = \sim 80$ Å. Interestingly, in the simulation, Arg^{17} maintained its interaction with the DNA of the neighboring NCP at $d = \sim 80$ Å even after the H4 tail-acidic patch interaction was lost (28). This indicates that the H4 tail can maintain the interaction with the DNA even when the H4 tail-acidic patch interaction is lost at $d = \sim 80$ Å. Consequently, we assume that the H4 tail-acidic patch interaction could be replaced by the H4 tail-DNA interaction in the single-molecule experiment at $d = \sim 80$ Å, and thus the force in the experiment would be similar to the calculated force of 15−18 pN. However, this value is ~4 times larger than the experimental value of 4.5 pN.

One reason for the difference may be because the linker DNA was not included in this study. The linker DNA that connects the neighboring NCPs adopts a stressed form, i.e., a bent and twisted conformation in the NCP array. This energetically unfavorable conformation of the linker DNA would be relaxed by the stretching of the NCP array. The repulsion between the negatively charged linker DNAs would also be relaxed. Therefore, the repulsive internucleosomal interaction that is derived from the linker DNA will counteract the attractive interaction between the NCPs by the H4 tail-bridge, which would result in the reduced value of 4.5 pN that was observed in the experiment.

Another reason for the difference may be because the H4 tail does not always interact with the acidic patch in the intraarray. A CG simulation of an NCP array of 24 nucleosomes showed that the H4 tails interacted with not only the acidic patch but also the DNA (23) (in the presence of 150 mM monovalent salt, 1 mM divalent salt, and linker histone). This indicates that the H4 tails exchange interaction with the acidic path and the DNA, during which the H4 tails would not strongly interact with the neighboring NCP and the force between the NCPs could be reduced to the calculated force of ~−3 to −7 pN. The CG simulation also showed that the time the H4 tails spent engaged in internucleosomal interactions with neighboring nucleosomes was ~30%, and with nonparental linker DNA, ~0%; whereas the time spent in intranucleosomal interactions with the parent nucleosome was ~40%, and with parental linker DNA, ~0%. The time spent in free interaction was ~30%. Assuming that the rate of the nucleosomal interactions is the same as that of the single stack of perpendicular nucleosomes in the experiment, the stretching force would be reduced to ~15−18 pN × 30% + ~−3 to −7 pN × 30%, which equals ~3–5 pN, within which the single-molecule mechanic measurement of 4.5 pN falls.

Consequently, the experimental data of the internucleosomal stretching would be the averaged value derived from many different conformations of the NCPs in the specific NCP array, where some NCPs have specific H4 tail-bridge interactions and others have nonspecific interactions without the H4 tails being involved.

Mechanism of structural polymorphism and dynamics of chromatin

In this study, the main contributor to the free energies for the separation of the NCPs was found to be the H4 tail-bridge. $Arg^{19}-Arg^{23}$ were involved in the interfacial interaction between the NCPs at $d = \sim 58-70$ Å. $Arg^{19}-Arg^{23}$ are likely to be involved in the internucleosomal interaction when the NCPs are close together. There are four Lys residues in the H4 tail that are known as sites of acetylation in vivo—Lys^5, Lys^8, Lys^{12}, and Lys^{16}. At least one residue of Lys^5, Lys^8,

and Lys^{12} was almost always involved in the H4 tail-bridge interaction in all the cases (Figs. 5 and S5). As residues $Ser^{1}-Lys^{12}$ can extend far enough to reach the neighboring NCP from their own NCP, it is likely that they are involved in the internucleosomal interaction when the NCPs are far apart. In this study, Lys^{16} between $Ser^{1}-Lys^{12}$ and $Arg^{19}-Arg^{23}$ acted as a pivot in opening the NCPs. Lys^{16} is known to be unique as the acetylation of Lys^{16} leads to the disruption of the intra-NCP-array interaction (52) or weakens the inter-NCP-array interaction (53), which cannot be simply explained by the charge neutralization. In the crystal structure that has a head-to-tail orientation (PDB: 1AOI (2)), $Lys^{16}-Arg^{23}$ interacted with the acidic patch of the neighboring NCP at $d = \sim 65-68$ Å. However, in the head-to-head orientation in our study, the interaction between $Lys^{16}-Arg^{23}$ and the acidic patch was not observed at any d. This indicates that H4 tail-acidic patch interaction may not be essential for the stability of the nucleosome stacking. The all-atom simulation of the two NCPs by Saurabh et al. (28) also showed that Lys^{16}, which interacted with the DNA not the acidic patch, was critical for the stability of the NCPs. Therefore, Lys^{16} would stabilize the NCP by interacting with either the DNA or the acidic patch according to the conformational change of the NCPs in the chromatin.

Chromatin is generally considered to have an irregular structure in vivo (54), although a regular structure can be present in specific cells (55) (for a review, see (54)). Our simulations suggest that $Ser^{1}-Lys^{12}$ may contribute to the formation of the irregular structure as the H4 tail-bridge is able to extend far enough to form a variety of internucleosomal interactions, as observed at $d > \sim 80$ Å. The irregular conformation would be facilitated when $Ser^{1}-Lys^{12}$ are dominant in the internucleosomal interaction that forms the long H4 tail-bridge, whereas the regular structure would be facilitated when $Arg^{19}-Arg^{23}$ are dominant in the internucleosomal interaction that forms the short H4 tail-bridge. Consequently, the variety of internucleosomal H4 tail-bridges would drive the NCPs to form the regular and irregular structures of chromatin according to different formations of the H4 tail-bridge.

Finally, we examined the change in the dynamics of the NCPs from the regular stacked conformation to the separated irregular conformation. The total mass-weighted mean square fluctuation (MSF) of $\sum_{\alpha \in \text{atoms}} m_\alpha \Delta \mathbf{r}_\alpha^2$ for each NCP was measured against d. Fig. 7 shows that the MSF of each of the regular stacked NCPs was no lower than that of each of the irregularly separated NCPs. Contrary to our expectation, the dynamics of the NCP in the stacked state was maintained to a similar extent to that in the separated state. Probably, some of the entropy loss of the translational and rotational movements of each NCP in the stacked form was compensated for by the fluctuation of the NCP itself (56). This observation that the stacked NCPs maintained the large dynamics would be consistent

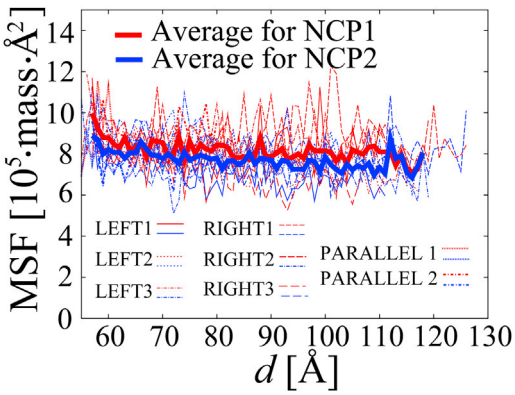

FIGURE 7 The total mass-weighted MSF for each NCP against d in LEFTs 1–3, RIGHTs 1–3, and PARALLELs 1–2. The averages of the total mass-weighted MSF for NCP_1 and NCP_2 for all the cases in the range of $d = 57$ to 119 Å are shown in thick red and blue lines, respectively. The coordinates of each NCP were best-fit in the rigid parts of the initial coordinate of each NCP (as defined for the calculation of the center of mass for each NCP). The unit is 10^5 atomic mass $Å^2$. To see this figure in color, go online.

with experimental data, which shows that the nucleosome arrays were intrinsically dynamic even when they were condensed (57), and that inactive compact chromatin (heterochromatin) remains dynamic (58).

Computational limitation

First, we simplified the model by truncating the H3 and H2B tails and by ignoring the connections between the 20-bp linker DNA. Thus, the NCPs are isolated in our system. Experimental data showed that the isolated NCPs were separated in solute at 150 mM NaCl (53) (at a pressure of one bar (14,15)), which is different from our observation that the stacked NCPs were stable at 150 mM NaCl. This may be interpreted that the state of the stabilized NCPs with strong H4 tail-bridge interaction in our system is a semistable one. Indeed, the free energy in RIGHT1 did not increase after two H4-tail bridges were lost, indicating that the free energy of 15−20 kcal/mol for separation would be much smaller if such strong H4 tail-bridges were not formed at $d = 58$ Å. Therefore, our system may represent a specific state of the stacked NCPs with the extremely strong H4 tail-bridge in the solution at 150 mM NaCl. In contrast, in the moderately folded NCP arrays at ~150 mM NaCl (6), there would exist a significant number of NCPs with the H4 tail-bridge. Our simulation evaluated the free energy of the NCPs from the stacked to separated state. Considering that our system did not include the positively charged H3 and H2B tails (and included the negatively charged 20-bp linker DNA), inclusion of these tails (and truncation of the 20-bp linker DNA) would further screen the DNA-DNA repulsion and stabilize the stacked NCPs. The possible involvement of the H3 tail-bridge and H2B tail-bridge

remains to be elucidated. Despite the limitation of this simplified model of the NCP array, the free energies for the different orientations of the NCPs obtained in our study can give insight into the understanding of the chromatin structure.

Second, to check whether the sampling of the H4 and H2A tails was sufficient, the convergence of the conformational entropies of the tails was calculated (Fig. S12; Table S3). In addition, the spatial distributions of the tails are shown in Fig. S13. Fig. S12 and Table S3 show that the conformational entropies did not converge in 20 ns in the umbrella sampling simulation but the increase every 5 ns became small after 20 ns. This indicates at least 25 ns of sampling is necessary to evaluate the entropy, because the location of the interaction between the H4 tail and the surface of the DNA frequently changed (Fig. S9). Although the entropies did not fully converge within 30 ns sampling, we do not think this would critically affect the accuracy of the free energy because the increase in the entropy appears uniform for the entire range of d considered and would become smaller during a longer simulation time.

CONCLUSIONS

The internucleosomal interactions between NCPs can be classified into three categories: 1) direct interfacial interaction between NCPs (d = from 58 to ~70 Å), which was estimated to be ~1−2 kcal/mol; 2) two bridge interactions between two H4 tails and the DNAs of the neighboring NCP (d = from 58 to ~70−89 Å) that prompt a variety of bridge interactions and promote diversity in the orientation of the NCPs; and 3) one left bridge interaction ($d >$ ~70−89 Å) in which the attractive force (from the bridge interaction and the electrostatic interaction between NCPs) was estimated to be ~15−18 pN per one H4 tail regardless of the different orientations of the NCPs and the different conformations of the H4 tails. The simulations of the NCPs without the H4 tails showed that the force between the NCPs was repulsive due to the electrostatic interaction between the DNAs, which confirmed the crucial role of the H4 tails in the attraction between the NCPs. The NCPs would open when the H4 tails are not involved in the formation of the H4 tail-bridge. Consequently, we concluded that the H4 tail plays a crucial role in a variety of internucleosomal interactions with the DNA of the spatially adjacent nucleosome, which would contribute to the polymorphism of the chromatin structure. In this study, H2B and H3 tails were not included, and the connection between the linker DNAs was ignored. Linker DNA would dominate the stability of the chromatin structure when the NCPs are spatially separated from each other because conformational stress in compact forms is relaxed. Nonetheless, this study suggests that the diversity of internucleosomal H4 tail-bridge interactions is essential in the polymorphic nature of the chromatin structure.

SUPPORTING MATERIAL

Supporting Materials and Methods, thirteen figures, and three tables are available at http://www.biophysj.org/biophysj/supplemental/S0006-3495(17)30813-5.

AUTHOR CONTRIBUTIONS

H.I. and H.K. designed the research. H.I. carried out all simulations, analyzed the data, and wrote the article. H.K. assisted in analyzing the data and writing the article.

ACKNOWLEDGMENTS

We thank Yvonne Ishida for reading this manuscript carefully.

This work was supported by the Ministry of Education, Culture, Sports, Science and Technology (MEXT) of Japan as "Priority Issue on Post-K Computer" (Building Innovative Drug Discovery Infrastructure Through Functional Control of Biomolecular Systems, Project IDs: hp160223 and hp170255), the HPCI system provided by Kyoto University (Project ID: hp170066) and Grants-in-Aid for Scientific Research from MEXT (JP25116003).

SUPPORTING CITATIONS

References (59,60) appear in the Supporting Material.

REFERENCES

1. Li, G., and D. Reinberg. 2011. Chromatin higher-order structures and gene regulation. *Curr. Opin. Genet. Dev.* 21:175–186.
2. Luger, K., A. W. Mäder, …, T. J. Richmond. 1997. Crystal structure of the nucleosome core particle at 2.8 Å resolution. *Nature*. 389:251–260.
3. Davey, C. A., D. F. Sargent, …, T. J. Richmond. 2002. Solvent mediated interactions in the structure of the nucleosome core particle at 1.9 Å resolution. *J. Mol. Biol.* 319:1097–1113.
4. Korolev, N., A. Allahverdi, …, L. Nordenskiöld. 2012. The polyelectrolyte properties of chromatin. *Soft Matter.* 8:9322–9333.
5. Korolev, N., A. P. Lyubartsev, and L. Nordenskiöld. 2010. Cation-induced polyelectrolyte-polyelectrolyte attraction in solutions of DNA and nucleosome core particles. *Adv. Colloid Interface Sci.* 158:32–47.
6. Allahverdi, A., Q. Chen, …, L. Nordenskiöld. 2015. Chromatin compaction under mixed salt conditions: opposite effects of sodium and potassium ions on nucleosome array folding. *Sci. Rep.* 5:8512.
7. Dorigo, B., T. Schalch, …, T. J. Richmond. 2003. Chromatin fiber folding: requirement for the histone H4 N-terminal tail. *J. Mol. Biol.* 327:85–96.
8. Gordon, F., K. Luger, and J. C. Hansen. 2005. The core histone N-terminal tail domains function independently and additively during salt-dependent oligomerization of nucleosomal arrays. *J. Biol. Chem.* 280:33701–33706.
9. Kan, P. Y., T. L. Caterino, and J. J. Hayes. 2009. The H4 tail domain participates in intra- and internucleosome interactions with protein and DNA during folding and oligomerization of nucleosome arrays. *Mol. Cell. Biol.* 29:538–546.
10. Pepenella, S., K. J. Murphy, and J. J. Hayes. 2014. A distinct switch in interactions of the histone H4 tail domain upon salt-dependent folding of nucleosome arrays. *J. Biol. Chem.* 289:27342–27351.

11. Dorigo, B., T. Schalch, …, T. J. Richmond. 2004. Nucleosome arrays reveal the two-start organization of the chromatin fiber. *Science.* 306:1571–1573.
12. Schalch, T., S. Duda, …, T. J. Richmond. 2005. X-ray structure of a tetranucleosome and its implications for the chromatin fibre. *Nature.* 436:138–141.
13. Frouws, T. D., H. G. Patterton, and B. T. Sewell. 2009. Histone octamer helical tubes suggest that an internucleosomal four-helix bundle stabilizes the chromatin fiber. *Biophys. J.* 96:3363–3371.
14. Leforestier, A., J. Dubochet, and F. Livolant. 2001. Bilayers of nucleosome core particles. *Biophys. J.* 81:2414–2421.
15. Livolant, F., S. Mangenot, A. Leforestier, A. Bertin, M. D. Frutos, E. Raspaud, and D. Durand. 2006. Are liquid crystalline properties of nucleosomes involved in chromosome structure and dynamics? *Philos. Trans. A Math. Phys. Eng. Sci.* 364:2615–2633.
16. Korolev, N., Y. Fan, …, L. Nordenskiöld. 2012. Modelling chromatin structure and dynamics: status and prospects. *Curr. Opin. Struct. Biol.* 22:151–159.
17. Kenzaki, H., N. Koga, …, S. Takada. 2011. CafeMol: a coarse-grained biomolecular simulator for simulating proteins at work. *J. Chem. Theory Comput.* 7:1979–1989.
18. Sambriski, E. J., D. C. Schwartz, and J. J. de Pablo. 2009. A mesoscale model of DNA and its renaturation. *Biophys. J.* 96:1675–1690.
19. Chang, L., and S. Takada. 2016. Histone acetylation dependent energy landscapes in tri-nucleosome revealed by residue-resolved molecular simulations. *Sci. Rep.* 6:34441.
20. Korolev, N., D. Luo, …, L. Nordenskiöld. 2014. A coarse-grained DNA model parameterized from atomistic simulations by inverse Monte Carlo. *Polymers.* 6:1655–1675.
21. Fan, Y., N. Korolev, …, L. Nordenskiöld. 2013. An advanced coarse-grained nucleosome core particle model for computer simulations of nucleosome-nucleosome interactions under varying ionic conditions. *PLoS One.* 8:e54228.
22. Wedemann, G., and J. Langowski. 2002. Computer simulation of the 30-nanometer chromatin fiber. *Biophys. J.* 82:2847–2859.
23. Arya, G., and T. Schlick. 2009. A tale of tails: how histone tails mediate chromatin compaction in different salt and linker histone environments. *J. Phys. Chem. A.* 113:4045–4059.
24. Kepper, N., R. Ettig, …, K. Rippe. 2011. Force spectroscopy of chromatin fibers: extracting energetics and structural information from Monte Carlo simulations. *Biopolymers.* 95:435–447.
25. Perišić, O., R. Collepardo-Guevara, and T. Schlick. 2010. Modeling studies of chromatin fiber structure as a function of DNA linker length. *J. Mol. Biol.* 403:777–802.
26. Collepardo-Guevara, R., G. Portella, …, M. Orozco. 2015. Chromatin unfolding by epigenetic modifications explained by dramatic impairment of internucleosome interactions: a multiscale computational study. *J. Am. Chem. Soc.* 137:10205–10215.
27. Zhang, R., J. Erler, and J. Langowski. 2017. Histone acetylation regulates chromatin accessibility: role of H4K16 in inter-nucleosome interaction. *Biophys. J.* 112:450–459.
28. Saurabh, S., M. A. Glaser, …, P. K. Maiti. 2016. Atomistic simulation of stacked nucleosome core particles: tail bridging, the H4 tail, and effect of hydrophobic forces. *J. Phys. Chem. B.* 120:3048–3060.
29. Kruithof, M., F.-T. Chien, …, J. van Noort. 2009. Single-molecule force spectroscopy reveals a highly compliant helical folding for the 30-nm chromatin fiber. *Nat. Struct. Mol. Biol.* 16:534–540.
30. Kono, H., K. Shirayama, …, H. Kurumizaka. 2015. Two arginine residues suppress the flexibility of nucleosomal DNA in the canonical nucleosome core. *PLoS One.* 10:e0120635.
31. Ikebe, J., S. Sakuraba, and H. Kono. 2016. H3 Histone tail conformation within the nucleosome and the impact of K14 acetylation studied using enhanced sampling simulation. *PLoS Comput. Biol.* 12:e1004788.
32. Li, Z., and H. Kono. 2016. Distinct roles of histone H3 and H2A tails in nucleosome stability. *Sci. Rep.* 6:31437.
33. Ishida, H., and S. Hayward. 2008. Path of nascent polypeptide in exit tunnel revealed by molecular dynamics simulation of ribosome. *Biophys. J.* 95:5962–5973.
34. Ishida, H. 2010. Branch migration of Holliday junction in RuvA tetramer complex studied by umbrella sampling simulation using a path-search algorithm. *J. Comput. Chem.* 31:2317–2329.
35. Ishida, H., and A. Matsumoto. 2014. Free-energy landscape of reverse tRNA translocation through the ribosome analyzed by electron microscopy density maps and molecular dynamics simulations. *PLoS One.* 9:e101951.
36. Ishida, H. 2014. Essential function of the N-termini tails of the proteasome for the gating mechanism revealed by molecular dynamics simulations. *Proteins.* 82:1985–1999.
37. Ishida, H., and A. Matsumoto. 2016. Mechanism for verification of mismatched and homoduplex DNAs by nucleotides-bound MutS analyzed by molecular dynamics simulations. *Proteins.* 84:1287–1303.
38. Hornak, V., R. Abel, …, C. Simmerling. 2006. Comparison of multiple Amber force fields and development of improved protein backbone parameters. *Proteins.* 65:712–725.
39. Pérez, A., I. Marchán, …, M. Orozco. 2007. Refinement of the AMBER force field for nucleic acids: improving the description of α/γ conformers. *Biophys. J.* 92:3817–3829.
40. Joung, I. S., and T. E. Cheatham, 3rd. 2008. Determination of alkali and halide monovalent ion parameters for use in explicitly solvated biomolecular simulations. *J. Phys. Chem. B.* 112:9020–9041.
41. Jorgensen, W. L., J. Chandrasekhar, …, M. L. Klein. 1983. Comparison of simple potential functions for simulating liquid water. *J. Chem. Phys.* 79:926–935.
42. Hockney, R. W., and J. W. Eastwood. 1988. Computer Simulation Using Particles. Adam Hilger, New York.
43. Deserno, M., and C. Holm. 1998. How to mesh up Ewald sums. I. A theoretical and numerical comparison of various particle mesh routines. *J. Chem. Phys.* 109:7678–7693.
44. Ryckaert, J., G. Cicotti, and H. J. C. Berendsen. 1977. Numerical integration of the Cartesian equations of motion of a system with constraints: molecular dynamics of *n*-alkanes. *J. Comput. Phys.* 23:327–341.
45. van Gunsteren, W. F., and H. J. C. Berendsen. 1977. Algorithms for macromolecular dynamics and constraint dynamics. *Mol. Phys.* 34:1311–1327.
46. Babin, V., C. Roland, and C. Sagui. 2008. Adaptively biased molecular dynamics for free energy calculations. *J. Chem. Phys.* 128:134101.
47. Raiteri, P., A. Laio, …, M. Parrinello. 2006. Efficient reconstruction of complex free energy landscapes by multiple walkers metadynamics. *J. Phys. Chem. B.* 110:3533–3539.
48. Kumar, S., D. Bouzida, …, J. M. Rosenberg. 1992. The weighted histogram analysis method for free energy calculations on biomolecules. I. the method. *J. Comput. Chem.* 13:1011–1021.
49. Schlitter, J. 1993. Estimation of absolute and relative entropies of macromolecules using the covariance matrix. *Chem. Phys. Lett.* 215:617–621.
50. Korolev, N., A. P. Lyubartsev, and L. Nordenskiöld. 2006. Computer modeling demonstrates that electrostatic attraction of nucleosomal DNA is mediated by histone tails. *Biophys. J.* 90:4305–4316.
51. Meng, H., K. Andresen, and J. van Noort. 2015. Quantitative analysis of single-molecule force spectroscopy on folded chromatin fibers. *Nucleic Acids Res.* 43:3578–3590.
52. Shogren-Knaak, M., H. Ishii, …, C. L. Peterson. 2006. Histone H4-K16 acetylation controls chromatin structure and protein interactions. *Science.* 311:844–847.
53. Liu, Y., C. Lu, …, L. Nordenskiöld. 2011. Influence of histone tails and H4 tail acetylations on nucleosome-nucleosome interactions. *J. Mol. Biol.* 414:749–764.
54. Maeshima, K., R. Imai, …, T. Nozaki. 2014. Chromatin as dynamic 10-nm fibers. *Chromosoma.* 123:225–237.

55. Woodcock, C. L. 1994. Chromatin fibers observed in situ in frozen hydrated sections. Native fiber diameter is not correlated with nucleosome repeat length. *J. Cell Biol.* 125:11–19.

56. Ishida, H., Y. Jochi, and A. Kidera. 1998. Dynamic structure of subtilisin-eglin *c* complex studied by normal mode analysis. *Proteins.* 32:324–333.

57. Poirier, M. G., E. Oh, …, J. Widom. 2009. Dynamics and function of compact nucleosome arrays. *Nat. Struct. Mol. Biol.* 16:938–944.

58. Bucceri, A., K. Kapitza, and F. Thoma. 2006. Rapid accessibility of nucleosomal DNA in yeast on a second time scale. *EMBO J.* 25:3123–3132.

59. Frishman, D., and P. Argos. 1995. Knowledge-based protein secondary structure assignment. *Proteins.* 23:566–579.

60. Pettersen, E. F., T. D. Goddard, …, T. E. Ferrin. 2004. UCSF Chimera—a visualization system for exploratory research and analysis. *J. Comput. Chem.* 25:1605–1612.

Biophysical Journal, Volume *113*

Supplemental Information

H4 Tails Potentially Produce the Diversity in the Orientation of Two Nucleosomes

Hisashi Ishida and Hidetoshi Kono

Supporting Material

H4 tails potentially produce the diversity in the orientation of two nucleosomes

Hisashi Ishida* and Hidetoshi Kono

Molecular Modeling and Simulation Group, Department of Quantum Beam Life Science, National Institutes for Quantum and Radiological Science and Technology, 8-1-7 Umemidai, Kizugawa, Kyoto 619-0215, Japan

* Corresponding author: ishida.hisashi@qst.go.jp

Simulated Annealing in vacuum

All the MD simulations were carried out using an MD simulation program called SCUBA (1-5) with the AMBER *ff*99SB (6), *ff*99bsc0 (7) and *ff*99ions08 (8) force-fields for histones, DNAs and ions, respectively. In order to optimize the conformation of the modelled tails, simulated annealing (SA) was performed in vacuum by assuming a distance-dependent dielectric constant of 4.0*r* with the value of *r* in Ångstrom. The van der Waals interactions were evaluated with a cut-off radius of 14 Å. All atoms of the modelled tails of the two NCPs were free to move but other heavy atoms of the histones and the DNA were restrained by harmonic restraints with a force constant of 10 kcal/mol/Å^2. Non-bonded interactions were evaluated with a cut-off radius of 12 Å. A time-step of 0.5 fs was used throughout the SA. The system was heated from 0 to 800 K during the first 50 ps and was then equilibrated for 50 ps. The equilibrated system was then gradually cooled for 400 ps from 800 K to 300 K. The SA was repeated 150 times and the resulting coordinate sets were stored as possible conformations of the tails at local minimum energy regions. Each of the 150 conformations was minimized for 500 steps using steepest descent followed by 5,000 steps of conjugate gradient. Then, the 63 lowest energy structures were selected as representatives of the two NCPs with H4 tails located in different positions. Here the energy considered was the total of the internal energy of the tails and the interaction energy between the tails and the two NCPs.

MD simulations of the systems in water

After the SA, the 63 structures were each placed in an aqueous medium. Each system of the two NCPs was placed in a rectangular box ~ 140 Å × 165 Å × 215 Å with the axis of the stacking of the two NCPs in the *z*-direction. In each box, all atoms of the two NCPs were separated more than 15 Å from the lateral edge of the box and 40 Å from the top edge of the box. To neutralize the charges of each system, sodium ions were placed at positions with large negative electrostatic potential. (438 Na^+ were used for neutralization.) Moreover, sodium and chloride ions were added to each box at random positions at a concentration of 150 mM NaCl. Then ~ 135,000 TIP3P water molecules (9) were added to surround each system. In total, each system comprised ~ 460,000 atoms.

To carry out energy minimization of all the systems to alleviate unfavorable interactions between the polymers and water molecules, steepest descent was performed for 500 steps, and conjugate gradient was performed for 5,000 steps. Harmonic restraints with a force constraint of 1.0 kcal/mol/Å^2 were applied to all the heavy atoms

of the molecules. The dielectric constant used was 1.0 and the van der Waals interactions were evaluated with a cut-off radius of 9 Å. The particle-particle particle-mesh (PPPM) method (10,11) was used for the electrostatic interactions for the direct space cutoff of 9 Å. For the PPPM calculations, charge grid sizes of 144 × 160 × 216 were chosen for the two NCPs system to set charge grid spacing close to 1 Å. The charge grid was interpolated using a spline of the order of seven, while the force was evaluated using a differential operator of the order of six (11).

All the systems were equilibrated at a constant pressure of one bar and a temperature of 300 K for 5 ns. The Langevin dynamics algorithm was utilized to control the temperature and pressure of the system. The coupling times for the temperature and pressure control were both set at 2 ps^{-1}. The SHAKE algorithm (12,13) was used to constrain all the bond lengths involving hydrogen atoms. The leap-frog algorithm with a time step of 2 fs was used throughout the simulation to integrate the equations of motion. Each system was first heated from 0 K to 300 K within 1 ns during which the molecules and sodium ions were fixed with decreasing restraints and the water molecules were allowed to move. After these the restraints were removed, the system was equilibrated for 10 ns at a constant pressure of one bar and a temperature of 300 K with no restraint. Then the box size was fixed, and an adaptively biased molecular dynamics (ABMD) simulation was carried out at a constant volume for all 63 structures with different initial coordinates of the H4 tails.

Adaptively Biased Molecular dynamics (ABMD) simulation

To observe the separation of the NCPs in the two NCPs, the ABMD method (14) combined with the multiple walker method (15) was employed in SCUBA. The equations of motion used in the ABMD method are expressed as (14):

$$\begin{aligned} m_a \frac{d^2\mathbf{r}_a}{dt^2} &= \mathbf{F}_a - \frac{\partial}{\partial \mathbf{r}_a} U\left[t \mid \sigma(\mathbf{R})\right], \\ \frac{\partial U(t \mid d)}{\partial t} &= \frac{k_B T}{\tau_F} K\left[d - \sigma(\mathbf{R})\right], \end{aligned} \qquad \text{(S1)}$$

where $\mathbf{R} \equiv (\mathbf{r}_1, ..., \mathbf{r}_N)$ are the coordinates of the NCP, and N is the number of atoms in the two NCPs. d is the reaction coordinate, and $\sigma(\mathbf{R})$ is a function to give the value of the reaction coordinate. k_B is the Boltzmann constant, T is the constant temperature, τ_F is the flooding time scale, and K is the kernel which has distribution around the reaction coordinate. The first equation is for atom a, with an additional force coming from the biasing potential $U(t|d)$ with an ordinary atomic force of $\boldsymbol{F_a}$. The second equation is

the time-evolving equation of the biasing potential. Details of the ABMD algorithm used in SCUBA are given in a reference (4).

The ABMD simulations were carried out at a constant volume and a temperature of 300K for 134 ns per system (a total of 8.4 μs for all 63 systems). The value of the reaction coordinate in the initial structure was 57.2 Å, and the range of the reaction coordinate for the ABMD simulations was set at $d \geq 50.0$ Å. The resolution of the reaction coordinate, Δd, was set at 1.0 Å. The relaxation time for the free-energy profile in Eq. (S1), τ, was set at 5000 ps. The two NCPs separated from each other in many systems as shown in Fig. 2. The conformation of the NCPs was stored every 1 ps for analysis.

Umbrella sampling simulations

Theoretically, for large enough τ_F and small enough width of the kernel, $U(t|d)$ converges towards the free-energy $F(d)$ times −1 as the simulation time elapses from $t = 0$ to ∞ (14). Using τ_F with a certain finite amount of time, the biasing potential (free-energy landscape times −1) fluctuates around the free-energy during the ABMD simulation (4,14). However, the biased potential did not show any fluctuation as shown in Fig. S1(a), indicating that the convergence of the free-energy is not accomplished. Moreover, as 63 systems moved to different conformations from each other as shown in Fig. 3, the identical biasing potential in our ABMD simulation would not be appropriate to represent possible different free-energies for each system. In this study, we paid attention to some models which we observed had distinctive orientations of the NCPs in the ABMD simulation, (LEFTs 1-3, RIGHTs 1-3 and PARALLELs 1-2 as shown in Fig. 3). Instead of continuing the ABMD simulation, we carried out umbrella sampling simulations of these models to obtain their free-energies.

The weighted histogram analysis method (WHAM) (16) was used to evaluate the free-energy from the sampled trajectories in the umbrella sampling simulations. In the WHAM approach, the unbiased probability distribution $P(\mathbf{R})$ is calculated from the biased probability distribution of the sampled coordinates as:

$$P(\mathbf{R}) = \sum_{i=1}^{N_{win}} n_i(\mathbf{R}) P_i^{(b)}(\mathbf{R}) \times \left[\sum_{j=1}^{N_{win}} n_j(\mathbf{R}) \exp\left(\left[F_j - V_j(\mathbf{R}) \right] / k_B T \right) \right]^{-1}, \qquad \text{(S2)}$$

where $\mathbf{R}$ is the atomic coordinates, N_{win} is the number of windows, $n_i(\mathbf{R})$ is the number of data points in the i-th window, $P_i^{(b)}(\mathbf{R})$ is a biased probability from the raw data obtained in the umbrella sampling simulation, $V_j(\mathbf{R})$ is the biasing potential in the j-th window, k_B is the Boltzmann constant, and T is the constant temperature. In this study,

$V_j(\mathbf{R})$ was selected to be the sum of a harmonic potential and the ABMD biasing potential in the final stage of the ABMD simulation, which has the form:

$$V_i(\mathbf{R}) = k_i\left(d(\mathbf{R}) - d_i^{\mathrm{fix}}\right)^2 + c\cdot\left(U_{abmd}\left(d(\mathbf{R})\right) - U_{abmd}\left(d_0\right)\right), \qquad \text{(S3)}$$

where $d(\mathbf{R})$ is the umbrella sampling coordinate, which was set to be $\sigma(\mathbf{R})$. d_i^{fix} is a fixed distance to sample umbrella coordinates of $d(\mathbf{R})$ around the desired position of d_i^{fix}. The initial coordinates of $\mathbf{R}$ for the i-th window were selected from the trajectories which had similar d_i^{fix} in the ABMD simulation. The values of d_i^{fix} were set from 58 Å to 110, 115 and 110 Å for LEFTs 1-3, 122, 118 and 105 Å for RIGHTs 1-3, 100 and 80 Å for PARALLELs 1-2, respectively, with intervals of 1 Å (i = 1,..., N_{win}). k_i is an arbitrary harmonic force constant, which was set at 0.2 kcal/mol/Å^2. U_{abmd} is the biasing potential at the final stage of the ABMD simulation (Fig. S1(a)). d_0 is a constant so that $U_{abmd}\left(d(\mathbf{R})\right) - U_{abmd}^0$ is zero at $d = d_0$. c is the arbitrary constant to scale U_{abmd}. If U_{abmd} were converged to the real free-energy landscape times -1, then $V_i(\mathbf{R})$ with k_i = 0.0 and c = 1.0 would let the NCPs behave like a random walk on the reaction coordinate of d. However, in an umbrella sampling simulation with c = 1.0, d monotonically drifted from the desired distance by ~ 3.0 Å on average for each window during each 10 ns (data not shown). This indicates that U_{abmd} at 134 ns overestimated the real free-energy. In contrast, using c = 0.0 shifted d from the desired position in a negative direction at $d \geq 60.0$ Å. In this study, c = 0.25 and 0.0 were used for $d > d_0$ and $d \leq d_0$ with d_0 = 60.0 Å, respectively. (More precisely, the biasing potential is expanded in terms of a third order B-spline function, and the coefficients of the B-spline function for $d \leq 60.0$ Å were set at zero. Therefore, the umbrella sampling potential is smoothly connected at d = 60.0 Å (see Fig. S1(b).) The initial atomic velocities were reset to eliminate the possibility of water convection by the separation of the NCPs during the ABMD simulation. The umbrella sampling simulation was carried out for 30 ns. The conformations of the NCPs was stored every 1 ps for analysis. The trajectory for the last 20 ns was used for the calculation of the free-energy landscape.

The coefficient F_j is defined by:

$$F_j = -k_B T \ln\left\{\sum_{\text{windows}} P(\mathbf{R})\exp\left(\left[-V_j(\mathbf{R})\right]/k_B T\right)\right\}, \quad (j = 1,\ldots N_{win}) \qquad \text{(S4)}$$

where the summation includes all the coordinates of **R** which were sampled over the total number of windows. By iterating Eqs. (S2) and (S4) to achieve self consistency (using a tolerance of 10^{-8}), the relative free-energy $F(\mathbf{R})$ at a given **R** is obtained as:

$$F(\mathbf{R}) = -k_B T \ln P(\mathbf{R}). \quad \text{(S5)}$$

To visualize the free-energy profile, the dimension of **R** in Eq. (S5) was reduced to 1 dimension by using the reaction coordinate, *d*.

The probability of the trajectories on *d*, $P(d)$, can be written as:

$$P(d) = \int P(\mathbf{R}')\delta(d - d')d\mathbf{R}', \quad \text{(S6)}$$

where $\delta(d)$ is the Dirac delta-function, and the free-energy profile in 1-dimension has the same form as Eq. (S5):

$$F(d) = -k_B T \ln P(d). \quad \text{(S7)}$$

To describe the changes in a physical quantity, *A*, such as the distance between atoms along *d*, the averaged quantity at *d*, $\bar{A}(d)$, is calculated by weighing the unbiased probability on the quantity $A(\mathbf{R})$ as:

$$\bar{A}(d) = \frac{\int A(\mathbf{R}')P(\mathbf{R}')\delta(d - d')d\mathbf{R}'}{P(d)}. \quad \text{(S8)}$$

The root mean square deviation (rmsd) from $\bar{A}(d)$ is calculated as:

$$\sqrt{\sigma^2(d)} = \sqrt{\overline{A^2}(d) - \bar{A}(d)^2} \quad \text{(S9)}$$

Umbrella sampling simulations of two NCPs without the H4 tails

To understand the role of the H4 tails, umbrella sampling simulations of two NCPs without the H4 tails were also carried out for LEFT 1, RIGHT 1 and PARALLEL 1 which had distinctive orientations of the NCP-NCP conformation. The initial atomic structure of the two NCPs without the H4 tails for each window was simply modeled by truncating the H4 tails (Ser1 to Ile 26) in the two NCPs which was used in the previous umbrella sampling simulations. To maintain the neutralization of the system, sodium ions were located at the positons of CZ atoms of Arg3, Arg17, Arg19, and Arg23, and NZ atoms of Lys5, Lys8, Lys12, Lys16, Lys20 in the H4 tails. Chloride ions were located at the positions of CG atoms of Asp24 in the H4 tails. An additional 172 × 4 water molecules were located at the positions of the other 172 × 4 heavy atoms of the four H4 tails to fill up the system. The system was minimized in the same way as

mentioned in “MD simulations of the systems in water”. Umbrella sampling simulations were carried out in the same way as mentioned in “Umbrella sampling simulations”, except for a longer simulation time of 40 ns with the last 20 ns analyzed. The arbitrary constant *c* in Eq. (S3) was set at zero for all the windows in the WHAM.

The conformational entropies of the H4 and H2A tails

The conformational entropies of the H4 and H2A tails were calculated using the quasiharmonic approximation (17) as follows:

$$S_{\mathrm{conf}} = 0.5\, k_B \ln \det [\mathbf{1}+(k_B T e^2/\hbar^2)\boldsymbol{\sigma}], \qquad \text{(S10)}$$

where *e* is *Euler*’s number, $\hbar$ is Planck’s constant divided by 2π. $\boldsymbol{\sigma} = < \boldsymbol{x}\, \boldsymbol{x}^{\mathrm{T}} >$ represents the mass-weighted covariance matrix, where $\boldsymbol{x}$ is the coordinates of the H4 $\mathrm{tail}_{1/2}$ (residues 1 to 26, 401 atoms) and the H2A $\mathrm{tail}_{1/2}$ (residues 1 to 17, 266 atoms). The trajectories in the *i*-th window of the umbrella sampling simulation where the desired position of d_i^{fix} was set in Eq. (S3) were used for the calculation of the conformational entropies to keep the number of sampled conformations the same for all d_i^{fix}. For the calculation of each covariance matrix for the H4 and H2A tails, $\boldsymbol{x}$ was best-fit in the reference coordinates. Each of the coordinates of the H4 and H2A $\mathrm{tails}_{1/2}$ in the initial structure in the *i*-th window of the umbrella sampling simulation was used as the reference coordinates for the best-fit at d_i^{fix}. (Hereafter, d_i^{fix} is referred to as d^{fix} unless it is specifically mentioned otherwise.) It should be noted that the conformational entropies calculated by the quasiharmonic approximation can be markedly overestimated because of the anharmonicity in protein dynamics (4).

SEQRES 1 I 347 DA DC DT DT DA DC DA DT DG DC DA DC DA

SEQRES 2 I 347 DG DG DA DT DG DT DA DA **DC=(Cyt22)$_1$** DC DT DG DC

SEQRES 3 I 347 DA DG DA DT DA DC DT DA DC DC DA DA DA

SEQRES 4 I 347 DA DG DT DG DT DA DT DT DT DG DG DA DA

SEQRES 5 I 347 DA DC DT DG DC DT DC DC DA **DT=(Thy62)$_1$** DC DA DA

SEQRES 6 I 347 DA DA DG DG DC DA DT DG DT DT DC DA DG

SEQRES 7 I 347 DC DT DG DG DA DT DT DC DC DA DG DC DT

SEQRES 8 I 347 DG DA DA DC DA DT DG DC DC DT DT DT DT

SEQRES 9 I 347 DG DA DT DG DG DA DG DC DA DG DT DT DT

SEQRES 10 I 347 DC DC DA DA DA DT DA DC DA DC DT DT DT

SEQRES 11 I 347 DT DG DG DT DA DG DT DA DT DC DT DG DC

SEQRES 12 I 347 DA DG DG DT DG DA DT DT DC DT DC DC DA

SEQRES 13 I 347 DG DG DG DC DG DG DC DC DA DG DT DA DC

SEQRES 14 I 347 DT DT DA DC DA DT DG DC DA DC DA DG DG

SEQRES 15 I 347 DA DT DG DT DA DA **DC=(Cyt189)$_2$** DC DT DG DC DA DG

SEQRES 16 I 347 DA DT DA DC DT DA DC DC DA DA DA DA DG

SEQRES 17 I 347 DT DG DT DA DT DT DT DG DG DA DA DA DC

SEQRES 18 I 347 DT DG DC DT DC DC DA **DT=(Thy229)$_2$** DC DA DA DA DA

SEQRES 19 I 347 DG DG DC DA DT DG DT DT DC DA DG DC DT

SEQRES 20 I 347 DG DG DA DT DT DC DC DA DG DC DT DG DA

SEQRES 21 I 347 DA DC DA DT DG DC DC DT DT DT DT DG DA

SEQRES 22 I 347 DT DG DG DA DG DC DA DG DT DT DT DC DC

SEQRES 23 I 347 DA DA DA DT DA DC DA DC DT DT DT DT DG

SEQRES 24 I 347 DG DT DA DG DT DA DT DC DT DG DC DA DG

SEQRES 25 I 347 DG DT DG DA DT DT DC DT DC DC DA DG DA

SEQRES 26 I 347 DC DT DT DA DC DA DT DG DC ~~DG DC DA DT~~

SEQRES 27 I 347 ~~DG DT DA DA DG DT DG DC DA~~

SEQRES 1 J 347 ~~DT DG DC DA DC DT DT DA DC DA DT DG DC~~

SEQRES 2 J 347 DG DC DA DT DG DT DA DA DG DT DC DT DG

SEQRES 3 J 347 DG DA DG DA DA DT DC DA DC DC DT DG DC

SEQRES 4 J 347 DA DG DA DT DA DC DT DA DC DC DA DA DA

SEQRES 5 J 347 DA DG DT DG DT DA DT DT DT DG DG DA DA

SEQRES 6 J 347 DA DC DT DG DC DT DC DC DA DT DC DA DA

SEQRES 7 J 347 DA DA DG DG DC DA DT DG DT DT DC DA DG

SEQRES 8 J 347 DC DT DG DG DA DA DT DC DC DA DG DC DT

SEQRES 9 J 347 DG DA DA DC DA DT DG DC DC DT DT DT DT

SEQRES 10 J 347 DG DA DT DG DG DA DG DC DA DG DT DT DT
SEQRES 11 J 347 DC DC DA DA DA DT DA DC DA DC DT DT DT
SEQRES 12 J 347 DT DG DG DT DA DG DT DA DT DC DT DG DC
SEQRES 13 J 347 DA DG DG DT DT DA DC DA DT DC DC DT DG
SEQRES 14 J 347 DT DG DC DA DT DG DT DA DA DG DT DA DC
SEQRES 15 J 347 DT DG DG DC DC DG DC DC DC DT DG DG DA
SEQRES 16 J 347 DG DA DA DT DC DA DC DC DT DG DC DA DG
SEQRES 17 J 347 DA DT DA DC DT DA DC DC DA DA DA DA DG
SEQRES 18 J 347 DT DG DT DA DT DT DT DG DG DA DA DA DC
SEQRES 19 J 347 DT DG DC DT DC DC DA DT DC DA DA DA DA
SEQRES 20 J 347 DG DG DC DA DT DG DT DT DC DA DG DC DT
SEQRES 21 J 347 DG DG DA DA DT DC DC DA DG DC DT DG DA
SEQRES 22 J 347 DA DC DA DT DG DC DC DT DT DT DT DG DA
SEQRES 23 J 347 DT DG DG DA DG DC DA DG DT DT DT DC DC
SEQRES 24 J 347 DA DA DA DT DA DC DA DC DT DT DT DT DG
SEQRES 25 J 347 DG DT DA DG DT DA DT DC DT DG DC DA DG
SEQRES 26 J 347 DG DT DT DA DC DA DT DC DC DT DG DT DG
SEQRES 27 J 347 DC DA DT DG DT DA DA DG DT

Table S1 The sequence of nucleotides in $DNA_{1/2}$ in the model of the two NCPs is shown in the following SEQRES comment in PDB 1ZBB (18);
DNA_1 (167 nucleotides of I-chain from sequence 1 to 167, shown in green)
DNA_2 (167 nucleotides of I-chain from sequence 168 to 334, shown in brown)
DNA_2 (167 nucleotides of J-chain from sequence 14 to 180, shown in blue)
DNA_1 (167 nucleotides of J-chain from sequence 181 to 347, shown in red)
(Nucleotides of I-chain from sequence 335 to 347 and nucleotides of J-chain from sequence 1 to 13 were truncated in our system.) The nucleotides of $(Cyt22)_1$, $(Thy62)_1$, $(Cyt189)_2$ and $(Thy229)_2$ which are shown in Fig. 1 are marked in bold.

	α-helix	3_{10}-helix	β-strand	turn	bridge	coil
LEFT 1	0.006 (0.040)	0.107 (0.274)	0.007 (0.036)	5.931 (1.835)	0.042 (0.096)	19.907 (1.912)
	0.002 (0.014)	0.039 (0.160)	0.000 (0.000)	7.038 (2.317)	0.025 (0.119)	18.895 (2.324)
	0.000 (0.000)	0.043 (0.199)	0.004 (0.019)	3.041 (0.019)	0.014 (0.044)	13.899 (1.633)
	0.001 (0.006)	0.013 (0.063)	0.005 (0.034)	7.968 (1.244)	0.051 (0.144)	8.963 (1.280)
LEFT 2	0.074 (0.244)	0.180 (0.433)	0.001 (0.005)	7.552 (1.914)	0.091 (0.209)	18.103 (1.959)
	0.039(0.206)	0.081 (0.254)	0.002 (0.015)	7.591 (2.589)	0.078 (0.246)	18.208 (2.583)
	0.000 (0.003)	0.321 (0.539)	0.007 (0.032)	4.877 (1.839)	0.064 (0.137)	11.731 (2.194)
	0.000 (0.000)	0.028 (0.103)	0.000 (0.000)	6.626 (1.507)	0.043 (0.122)	10.303 (1.527)
LEFT 3	0.027 (0.101)	0.558 (0.706)	0.032 (0.099)	6.618 (2.165)	0.362 (0.493)	18.404 (2.199)
	0.022 (0.113)	0.192 (0.113)	0.071 (0.292)	6.367 (2.089)	0.413 (0.448)	18.931 (2.373)
	0.000 (0.000)	0.170 (0.442)	0.011 (0.036)	6.530 (1.499)	0.151 (0.279)	10.137 (1.624)
	0.003 (0.020)	0.114 (0.319)	0.004 (0.029)	5.258 (2.042)	0.100 (0.293)	11.521 (2.265)
RIGHT 1	0.001 (0.009)	0.188 (0.427)	0.465 (0.970)	7.063 (2.657)	0.615 (0.549)	17.668 (2.570)
	0.008 (0.039)	0.631 (0.768)	0.158 (0.630)	8.404 (2.119)	0.302 (0.360)	16.497 (2.298)
	0.000 (0.000)	0.001 (0.009)	0.000 (0.000)	1.122 (1.248)	0.007 (0.056)	15.870 (1.264)
	0.016 (0.130)	0.084 (0.213)	0.003 (0.013)	5.913 (1.604)	0.049 (0.114)	10.935 (1.674)
RIGHT 2	0.001 (0.005)	0.162 (0.414)	0.185 (0.453)	6.723 (2.207)	0.485 (0.475)	18.445 (2.389)
	0.001 (0.007)	0.269 (0.279)	0.007 (0.033)	7.280 (2.021)	0.263 (0.379)	18.178 (2.113)
	0.000 (0.000)	0.070 (0.183)	0.000 (0.000)	4.480 (1.530)	0.018 (0.116)	12.431 (1.618)
	0.022 (0.168)	0.119 (0.344)	0.011 (0.052)	3.013 (1.630)	0.073 (0.262)	13.762 (1.846)
RIGHT 3	0.009 (0.037)	0.093 (0.192)	0.000 (0.000)	4.007 (2.521)	0.019 (0.084)	21.872 (2.647)
	0.004 (0.029)	0.140 (0.412)	1.895 (2.449)	6.850 (2.140)	0.283 (0.370)	16.827 (3.752)
	0.000 (0.000)	0.069 (0.179)	0.057 (0.176)	4.062 (1.345)	0.401 (0.406)	12.410 (1.337)
	0.000 (0.000)	0.248 (0.575)	0.005 (0.020)	6.476 (1.310)	0.105 (0.203)	10.166 (1.481)
PARALLEL 1	0.023 (0.120)	0.237 (0.439)	0.001(0.006)	4.917 (1.918)	0.091 (0.163)	20.731 (2.051)
	0.055 (0.130)	0.049 (0.130)	0.066 (0.187)	6.396 (2.273)	0.297 (0.443)	19.137 (2.504)
	0.000 (0.000)	0.134(0.234)	0.032 (0.078)	5.079 (0.715)	0.293 (0.173)	11.462 (0.699)
	0.041 (0.090)	0.115 (0.146)	0.006 (0.018)	4.422 (0.883)	0.095 (0.126)	12.321 (0.971)
PARALLEL 2	0.000 (0.000)	0.027 (0.072)	0.015 (0.037)	4.213 (1.559)	0.124 (0.236)	21.620 (1.696)
	0.000 (0.000)	0.437 (0.567)	0.002 (0.008)	7.945 (2.499)	0.244 (0.340)	17.373 (2.869)
	0.000 (0.000)	0.040 (0.117)	0.000 (0.000)	2.797 (2.045)	0.016 (0.047)	14.147 (2.085)
	0.000 (0.000)	0.000 (0.000)	0.002 (0.008)	4.443 (1.311)	0.545 (0.509)	12.011 (1.621)

Table S2 The average of a series of average numbers of residues forming secondary structures (α-helix, 3_{10}-helix, β-strand, turn, bridge and coil) along *d* in the 26-residue of the H4 tails 1 and 2 are shown in the first row (in red) and in the second row (in black), respectively. The value in brackets is the root-mean-square-deviation of a series of average numbers of the secondary structures.

	5ns	10ns	15ns	20ns	25ns	30ns
LEFT 1	0.854 (0.074)	0.911 (0.077)	0.943 (0.079)	0.974 (0.020)	0.990 (0.008)	1.000 (0.000)
	0.846 (0.069)	0.909 (0.071)	0.940 (0.073)	0.973 (0.018)	0.989 (0.007)	1.000 (0.000)
	0.873 (0.040)	0.925 (0.040)	0.950 (0.040)	0.978 (0.014)	0.991 (0.007)	1.000 (0.000)
	0.886 (0.034)	0.935 (0.030)	0.960 (0.026)	0.980 (0.016)	0.993 (0.007)	1.000 (0.000)
LEFT 2	0.875 (0.026)	0.931 (0.024)	0.961 (0.018)	0.980 (0.010)	0.992 (0.005)	1.000 (0.000)
	0.856 (0.032)	0.913 (0.025)	0.952 (0.015)	0.976 (0.008)	0.991 (0.004)	1.000 (0.000)
	0.885 (0.036)	0.936 (0.025)	0.964 (0.020)	0.982 (0.015)	0.993 (0.007)	1.000 (0.000)
	0.890 (0.034)	0.942 (0.025)	0.967 (0.017)	0.984 (0.009)	0.994 (0.005)	1.000 (0.000)
LEFT 3	0.864 (0.025)	0.927 (0.021)	0.957 (0.017)	0.976 (0.012)	0.990 (0.006)	1.000 (0.000)
	0.853 (0.031)	0.916 (0.024)	0.950 (0.018)	0.972 (0.013)	0.989 (0.007)	1.000 (0.000)
	0.892 (0.035)	0.942 (0.025)	0.964 (0.016)	0.982 (0.011)	0.993 (0.006)	1.000 (0.000)
	0.891 (0.029)	0.938 (0.023)	0.965 (0.015)	0.981 (0.011)	0.992 (0.006)	1.000 (0.000)
RIGHT 1	0.862 (0.028)	0.921 (0.025)	0.954 (0.019)	0.974 (0.014)	0.989 (0.008)	1.000 (0.000)
	0.860 (0.028)	0.921 (0.021)	0.953 (0.015)	0.976 (0.010)	0.991 (0.005)	1.000 (0.000)
	0.890 (0.027)	0.928 (0.021)	0.954 (0.016)	0.979 (0.014)	0.989 (0.007)	1.000 (0.000)
	0.872 (0.033)	0.927 (0.031)	0.957 (0.023)	0.976 (0.014)	0.992 (0.007)	1.000 (0.000)
RIGHT 2	0.855 (0.032)	0.920 (0.021)	0.953 (0.013)	0.974 (0.011)	0.990 (0.006)	1.000 (0.000)
	0.854 (0.029)	0.919 (0.020)	0.952 (0.016)	0.974 (0.011)	0.990 (0.006)	1.000 (0.000)
	0.894 (0.028)	0.943 (0.021)	0.969 (0.015)	0.983 (0.012)	0.993 (0.007)	1.000 (0.000)
	0.881 (0.035)	0.935 (0.022)	0.965 (0.015)	0.982 (0.010)	0.993 (0.006)	1.000 (0.000)
RIGHT 3	0.857 (0.027)	0.915 (0.023)	0.946 (0.021)	0.971 (0.012)	0.989 (0.006)	1.000 (0.000)
	0.852 (0.035)	0.912 (0.030)	0.942 (0.027)	0.968 (0.014)	0.988 (0.008)	1.000 (0.000)
	0.881 (0.034)	0.927 (0.036)	0.950 (0.036)	0.977 (0.014)	0.992 (0.006)	1.000 (0.000)
	0.890 (0.038)	0.940 (0.025)	0.965 (0.021)	0.983 (0.014)	0.993 (0.008)	1.000 (0.000)
PARALLEL 1	0.863 (0.020)	0.921 (0.017)	0.953 (0.012)	0.973 (0.008)	0.989 (0.004)	1.000 (0.000)
	0.855 (0.030)	0.917 (0.024)	0.950 (0.016)	0.972 (0.012)	0.989 (0.007)	1.000 (0.000)
	0.888 (0.028)	0.936 (0.026)	0.965 (0.016)	0.980 (0.011)	0.992 (0.008)	1.000 (0.000)
	0.881 (0.033)	0.931 (0.026)	0.958 (0.022)	0.974 (0.017)	0.988 (0.011)	1.000 (0.000)
PARALLEL 2	0.870 (0.032)	0.922 (0.028)	0.954 (0.021)	0.974 (0.017)	0.989 (0.008)	1.000 (0.000)
	0.851 (0.035)	0.906 (0.028)	0.945 (0.024)	0.972 (0.014)	0.987 (0.009)	1.000 (0.000)
	0.904 (0.034)	0.941 (0.025)	0.965 (0.016)	0.983 (0.008)	0.994 (0.005)	1.000 (0.000)
	0.902 (0.039)	0.940 (0.035)	0.963 (0.026)	0.980 (0.019)	0.992 (0.008)	1.000 (0.000)

Table S3 The average ratios of the conformational entropies of the H4 tails$_{1/2}$ and H2A tails$_{1/2}$ for 5 ns (from 10 to 15 ns), 10 ns (from 10 to 20 ns), 15 ns (from 10 to 25 ns), 20 ns (from 10 to 30 ns), 25 ns (from 5 to 30 ns) and 30 ns (from 0 to 30 ns) of the umbrella sampling simulations are listed in the first/second (in red) and third/fourth (in black) rows, respectively. The value in brackets is the root-mean-square-deviation of the ratios.

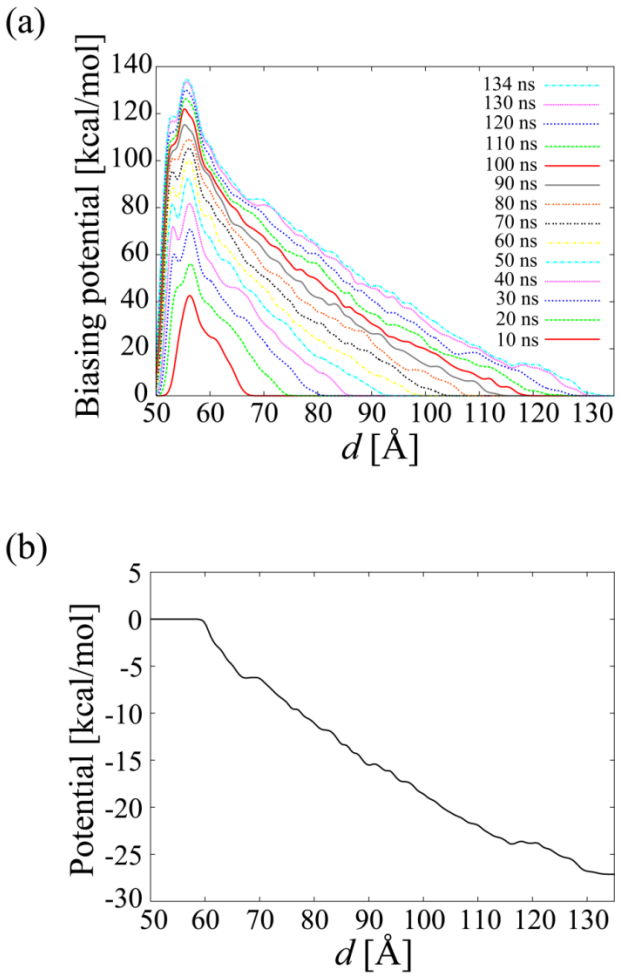

Fig. S1 (a) The evolution of the biasing potential (b) the biasing potential of the second term in Eq. (S3) (or Eq. (3)) used for the umbrella sampling simulations

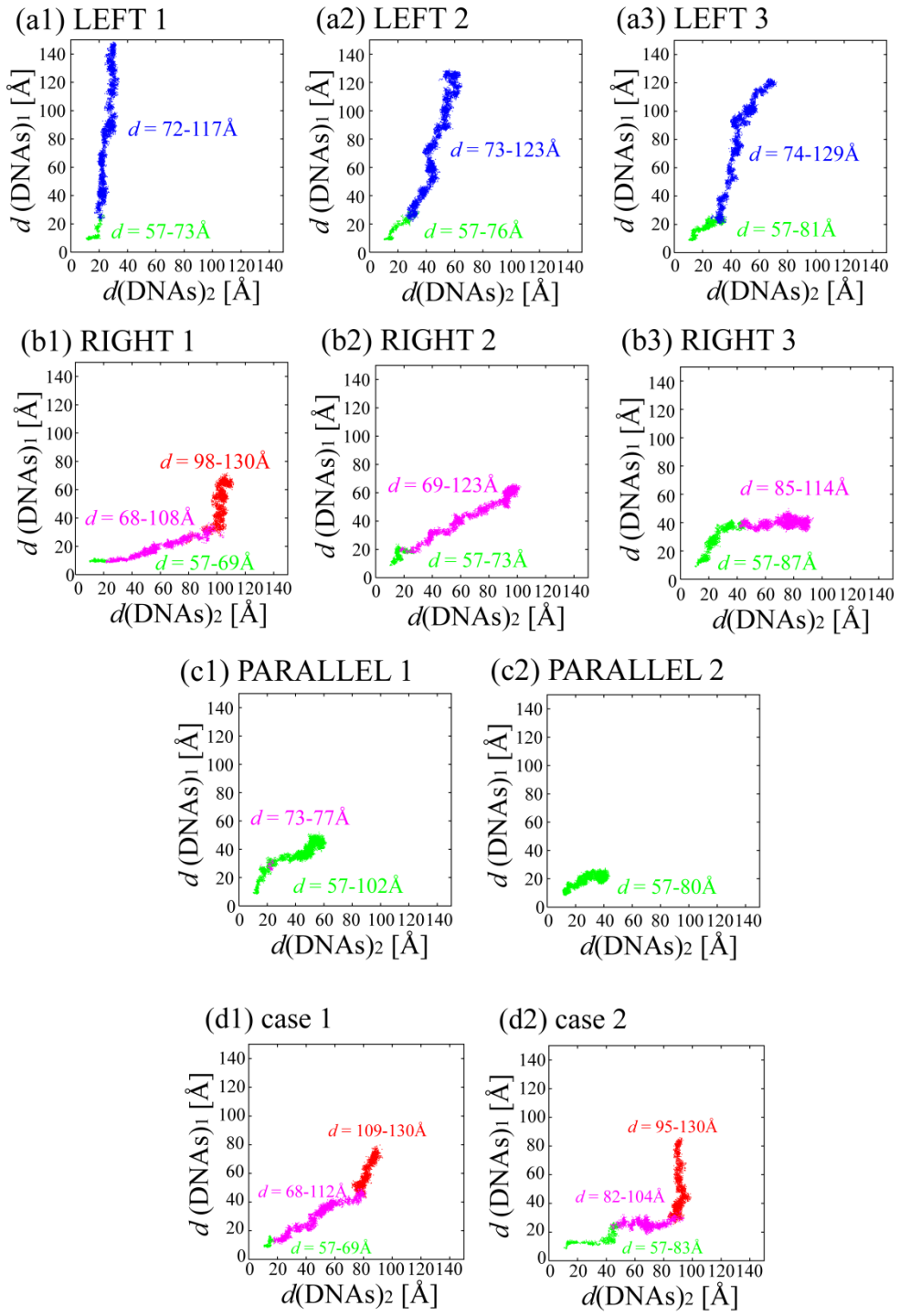

Fig. S2 The trajectories of $d(\mathrm{DNAs})_{2/1}$ of the eight selected models: (a) LEFTs 1-3, (b) RIGHTs 1-3, (c) PARALLELs 1-2 and (d) cases 1-2 which had the breakages of both of the $\mathrm{H4}_{2/1}$ tails, respectively The coloring is the same as that in Fig. 2. The ranges of *d* for each H4 tail-bridge formation are shown in the same color.

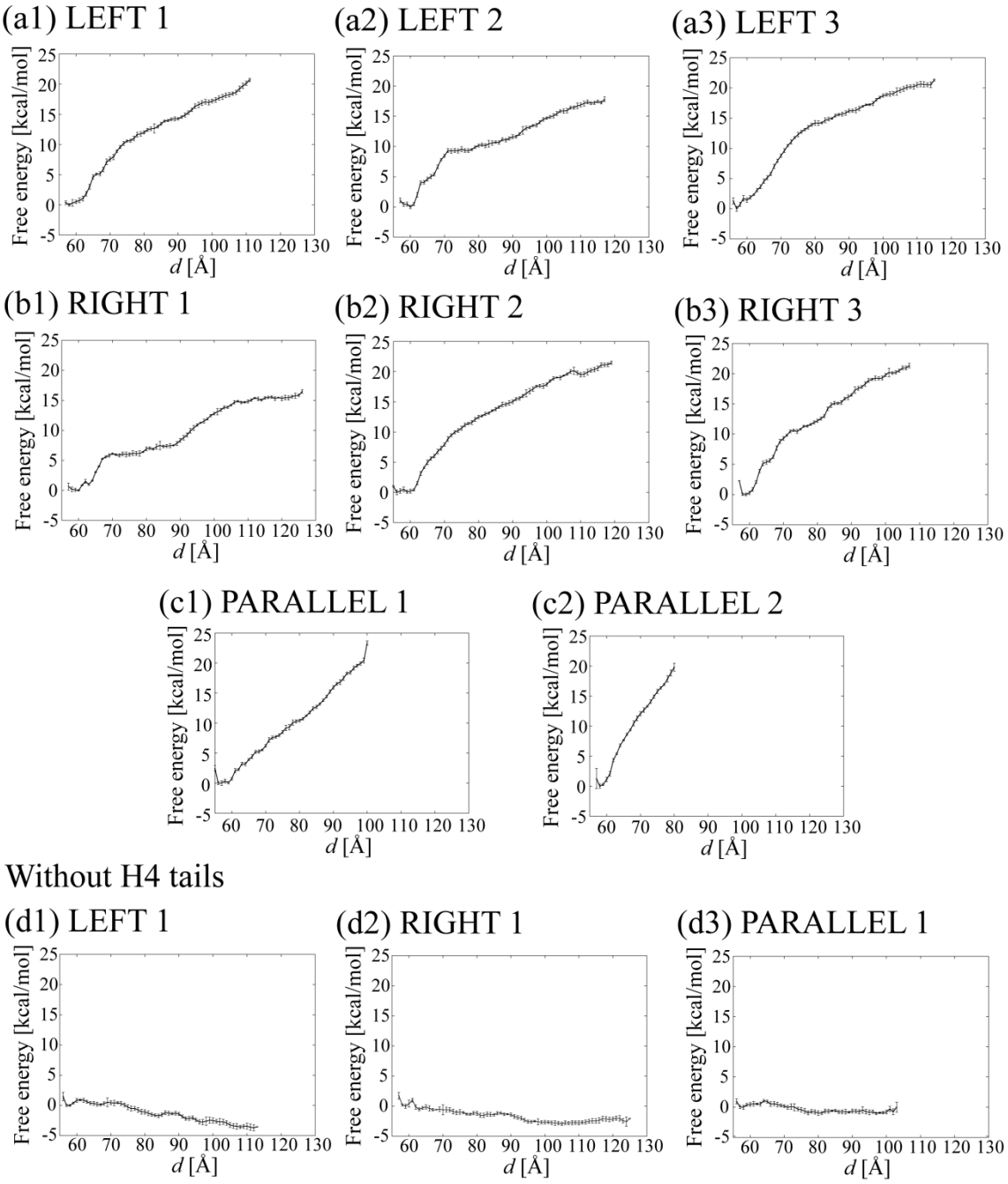

Fig. S3 Errors in the free-energies in (a) LEFTs 1-3, (b) RIGHTs 1-3, (c) PARALLELEs 1-2 and (d) RIGHT 1, LEFT 1 and PARALLEL 1 without the H4 tails. The root mean square errors (RMSEs) in the free-energies were determined by calculating free-energies for four non-overlapping segments (from 0 to 5 ns, from 5 to 10ns, 10 to 15 ns, and 15 to 20) of the 20 ns trajectory of the umbrella sampling simulations. Each free-energy which was calculated from a 5 ns trajectory was aligned to the final free-energy which was calculated from the 20 ns trajectory so that the

average of the free-energy coincides with the average of the final free-energy. To calculate the average of the free-energy, the values of the free-energy at *d* which were estimated using sufficient sampling data (more than 1% of the number of data points (20,000) for each segment in the window) were used; as for the NCPs with the H4 tails, in the range of *d* = 57 to 110 Å in LEFT 1, 57 to 117 Å in LEFT 2, and 57 to 114 Å in LEFT 3, 57 to 126 Å in RIGHT1, 56 to 119 Å in RIGHT2, 58 to 107 Å in RIGHT3, 56 to 99 Å in PARALLEL 1 and 58 to 80 Å in PARALLEL2. As for the NCPs without the H4 tails, in the range of *d* = 57 to 112 Å in LEFT 1, 57 to 124 Å in RIGHT 1, and 56 to 102 Å in PARALELL 1.

The RMSE for each system was calculated using the equation, $\sqrt{\sum_{k=1}^{n}\left(f_k(d)-\bar{f}\right)^2/(n-1)}$, where $f_k(d)$ is the value of the aligned free-energy at *d* and $\bar{f}$ is the average and *n* is the number of segments at *d* for each system (n is usually 4 except at *d* where sampling data is scarce). The RMSEs are shown in error bars along the final free-energy. The averages of the errors in the free-energies of the NCPs with H4 tails along *d* (within the range of sufficient sampling data) were 0.33, 0.30 and 0.31 kcal/mol in LEFTs 1-3, 0.25, 0.30 and 0.28 kcal/mol RIGHTs 1-3, 0.26 and 0.30 kcal/mol in PARALLELs 1-2, respectively. The errors in the free-energies of the NCPs without H4 tails were 0.34, 0.31 and 0.32 kcal/mol in LEFT 1, RIGHT 1, and PARALELL 1, respectively. The units of the free-energy and error are kcal/mol.

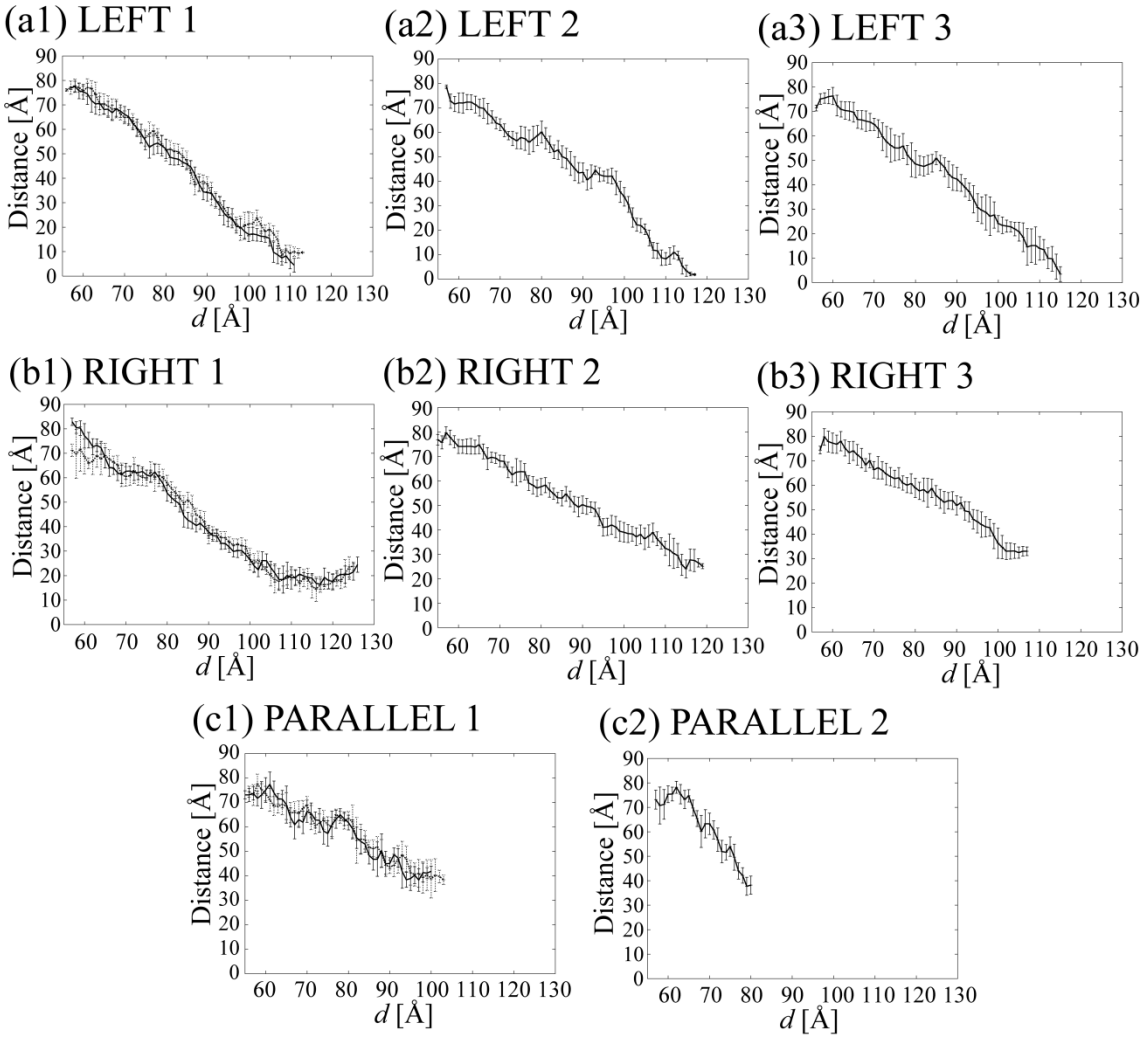

Fig. S4 The distance in the *z*-direction between NCP_1 in the system and NCP_2 in the mirror image in (a) LEFTs 1-3, (b) RIGHTs 1-3 and (c) PARALLELs 1-2. Each distance in LEFTs 1-3, RIGHTs 1-3 and PARALLELs 1-2 with the H4 tails is shown by a solid line, and each distance in LEFT 1, RIGHT 1 and PARALLEL 1 without the H4 tails is shown by a dotted line. The unit is Å.

(a1) LEFT 1

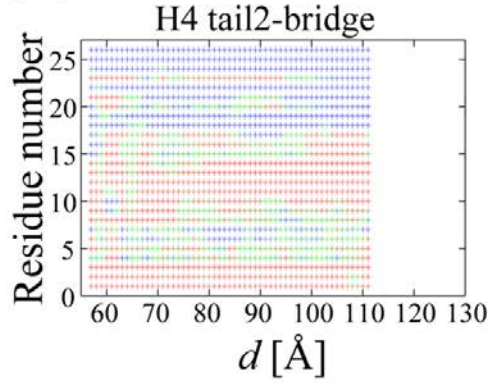

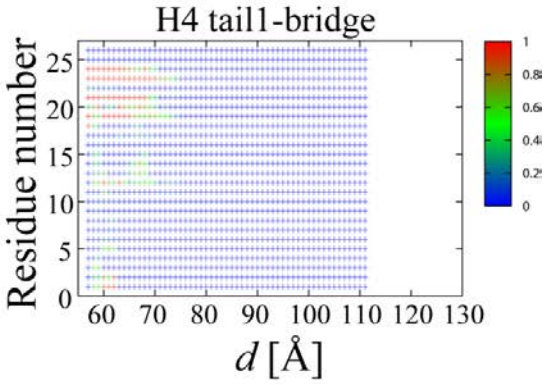

(a2) LEFT 2

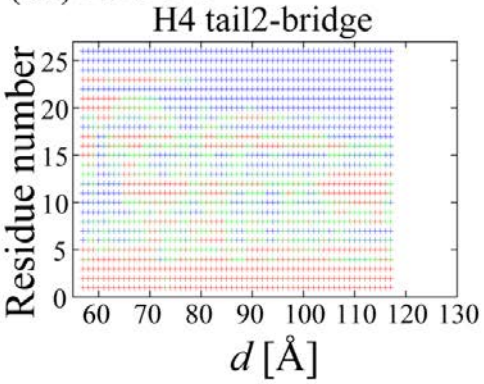

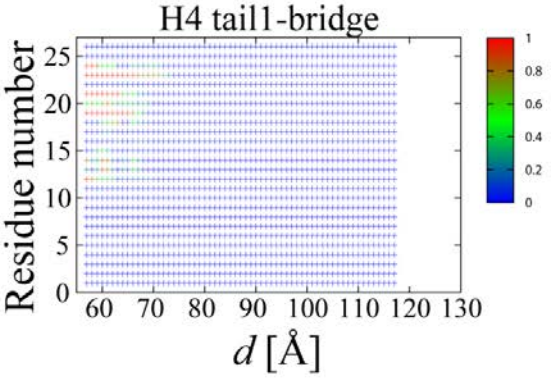

(a3) LEFT 3

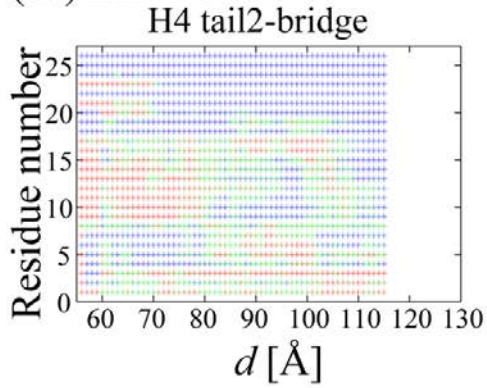

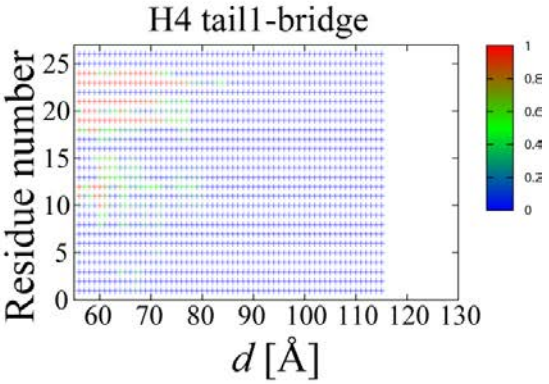

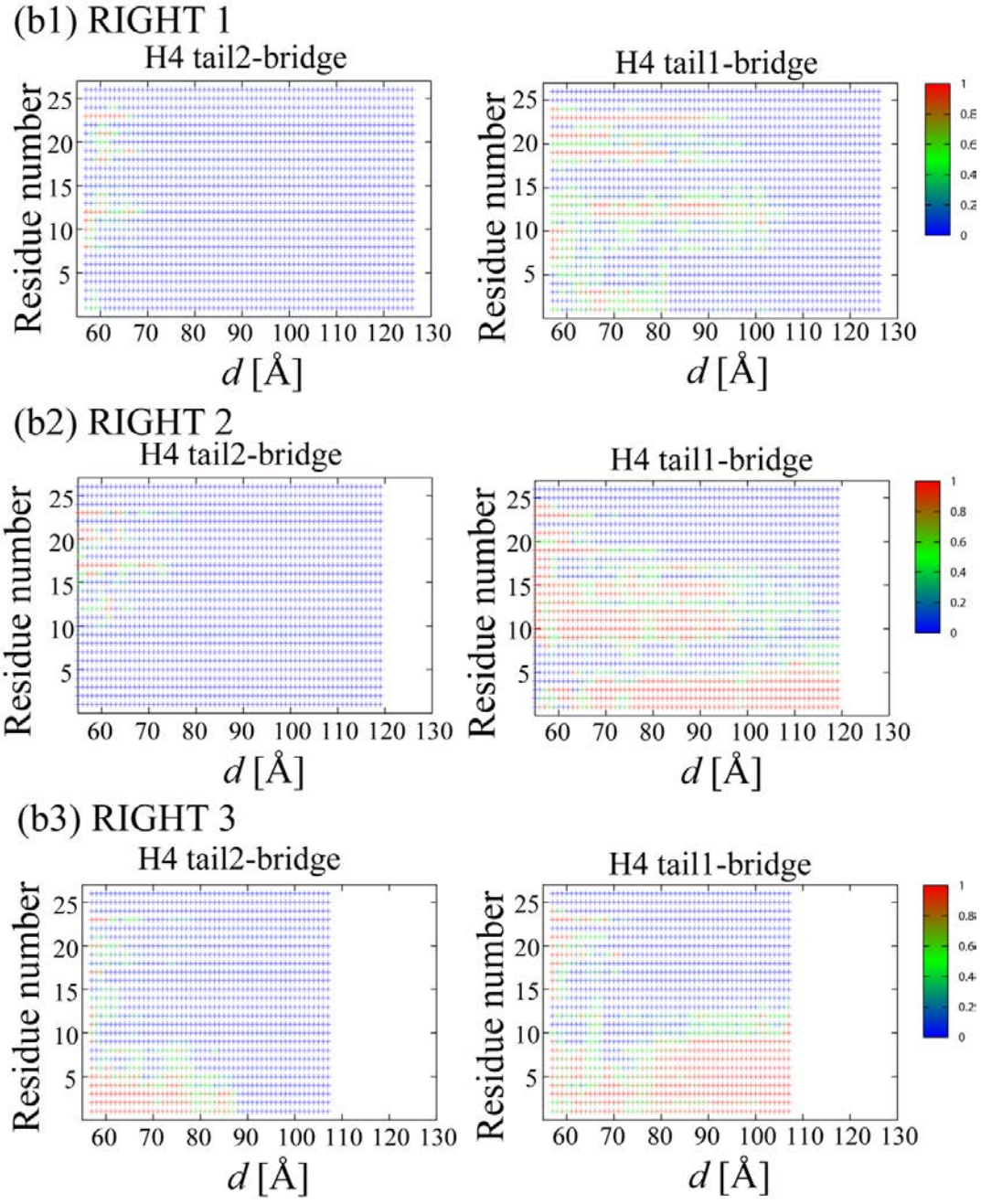
(b1) RIGHT 1
H4 tail2-bridge
H4 tail1-bridge
Residue number
d [Å]
(b2) RIGHT 2
H4 tail2-bridge
H4 tail1-bridge
Residue number
d [Å]
(b3) RIGHT 3
H4 tail2-bridge
H4 tail1-bridge
Residue number
d [Å]

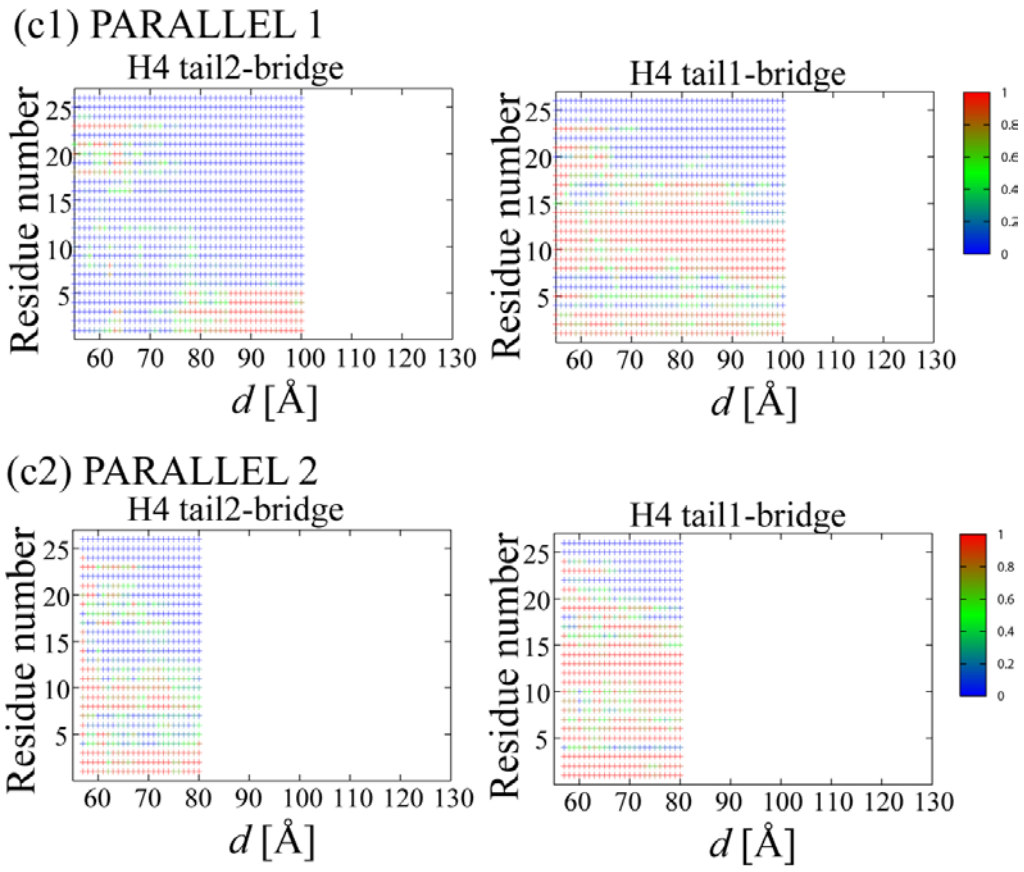

Fig. S5 The average population of residues which participated in the formation of H4 $tail_{1/2}$-bridge in (a) LEFTs 1-3, (b) RIGHTs 1-3 and (c) PARALLELs 1-2. The average was calculated according to Eq. (S8).

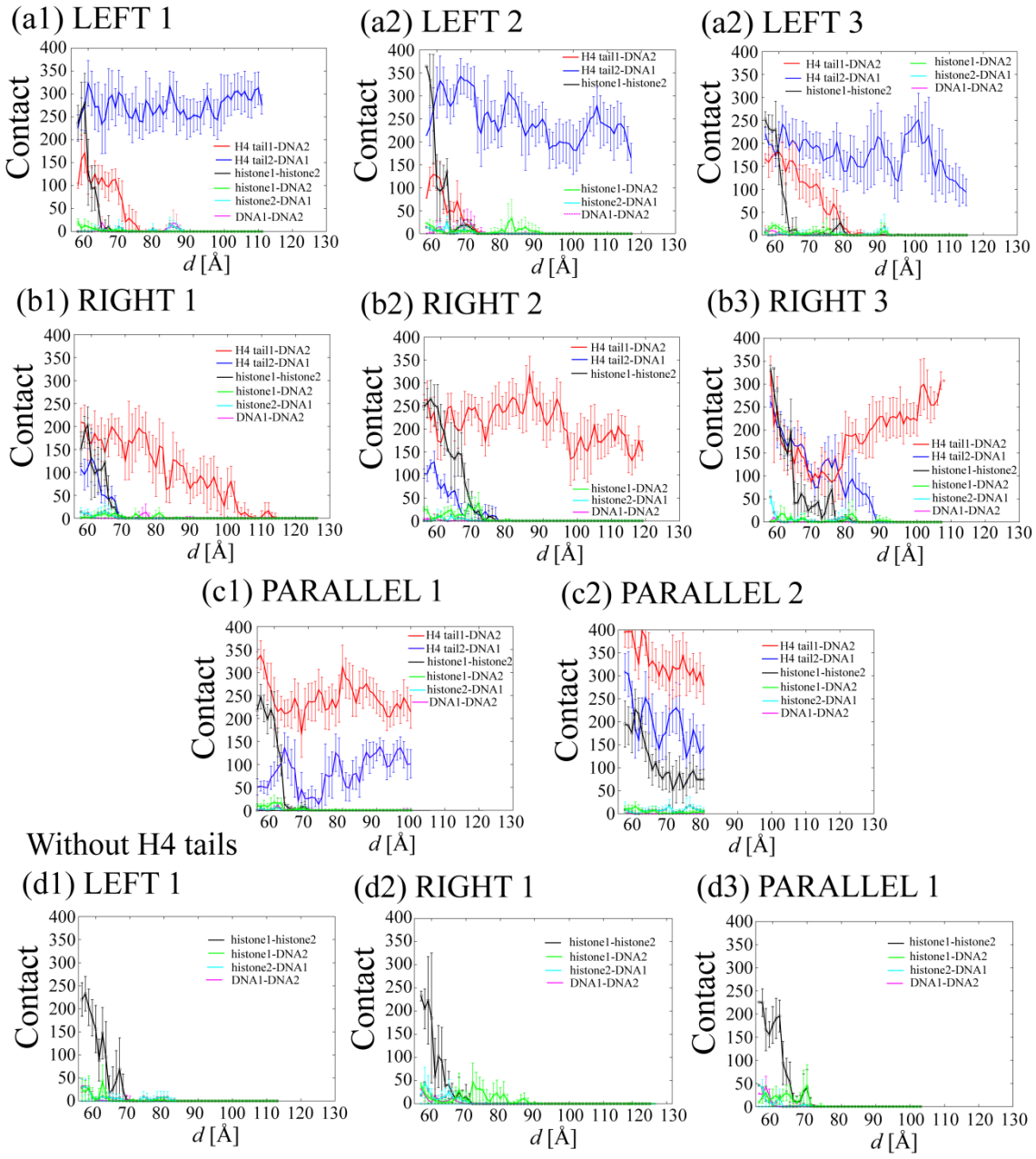

Fig. S6 The number of contacts between the NCPs (H4 $tail_{1/2}$ – $DNA_{2/1}$, $histone_1$ – $histone_2$ (excluding the H4 tails), $histone_{1/2}$ – $DNA_{2/1}$ and DNA_1 – DNA_2) in (a) LEFTs 1-3, (b) RIGHTs 1-3, (c) PARALLELs 1-2 and (d) RIGHT 1, LEFT 1 and PARALLEL 1 without the H4 tails. The contacts between H4 $tail_{1/2}$ and $histone_{2/1}$ were not observed in this study.

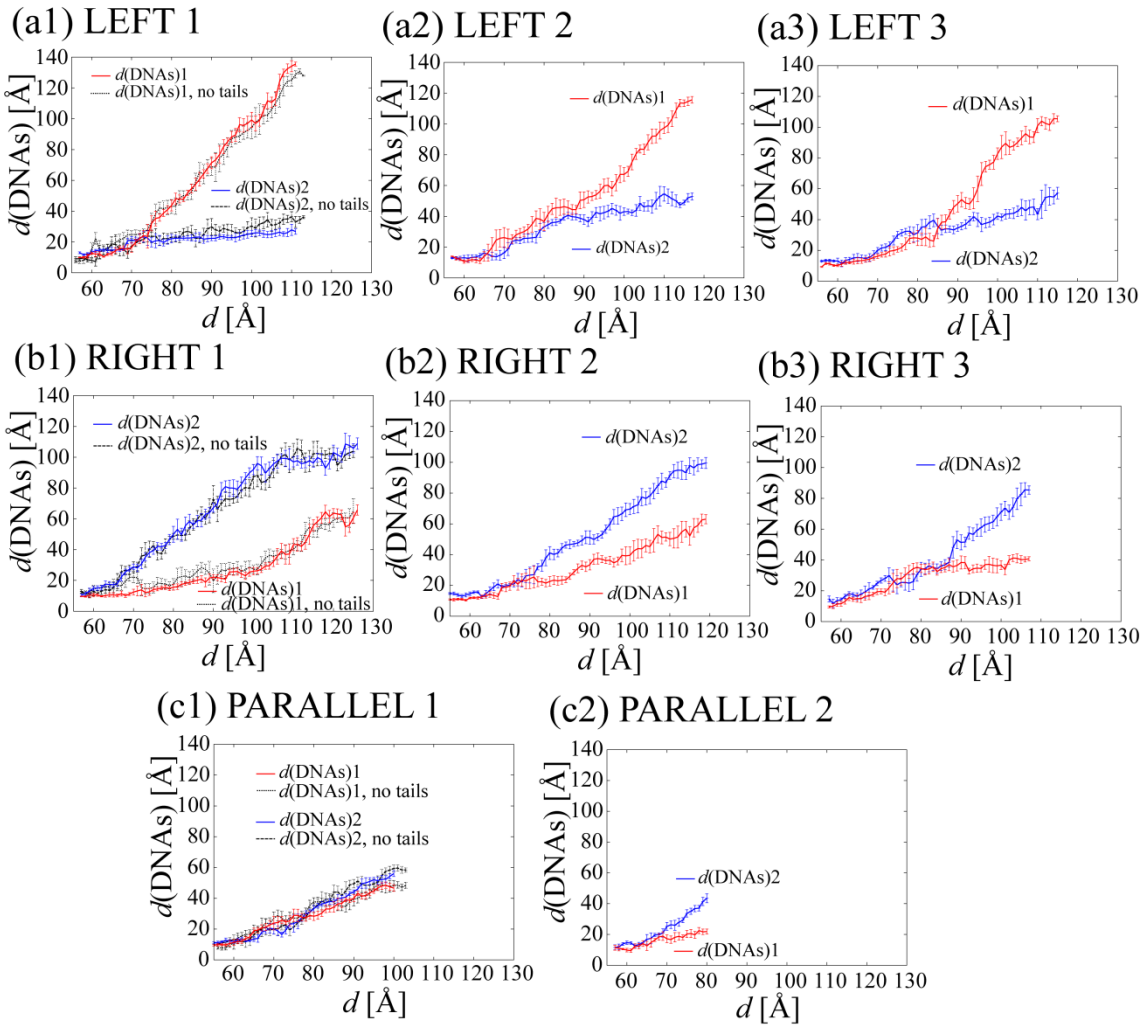

Fig. S7 $d(\mathrm{DNAs})_{2/1}$ against d for (a) LEFTs 1-3, (b) RIGHTs 1-3and (c) PARALLELs 1-2. The average and RMSD were calculated according to Eqs. (S8) and (S9), respectively.

(a1) LEFT 1

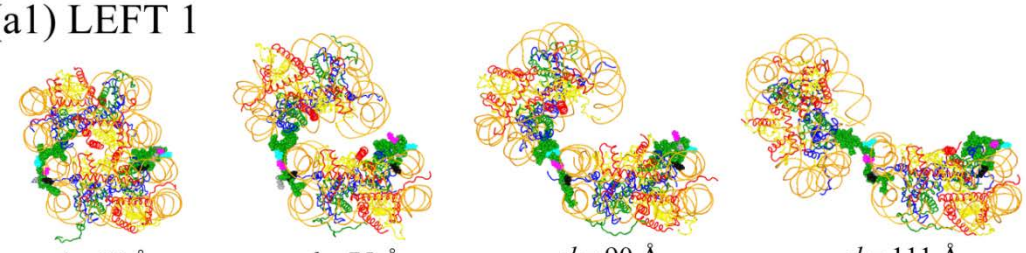

d = 58 Å (12.5 / 10.8 Å)

d = 75 Å (19.5 / 32.0 Å)

d = 90 Å (22.4 / 71.5 Å)

d = 111 Å (26.4 / 136.6 Å)

(a2) LEFT 1 (without H4 tails)

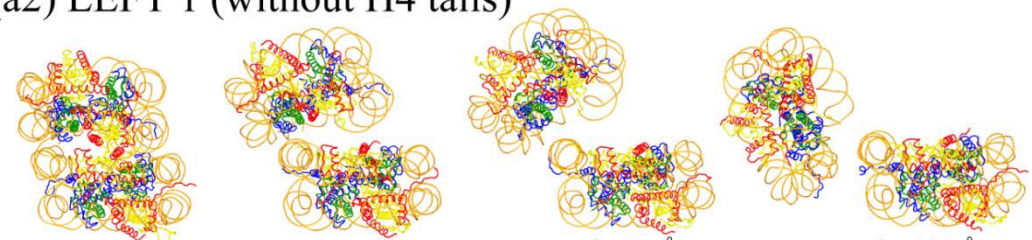

d = 58 Å (9.5 / 7.3 Å)

d = 75 Å (23.0 / 31.6 Å)

d = 90 Å (28.8 / 68.5 Å)

d = 111 Å (34.0 / 129.6 Å)

(a3) LEFT 2

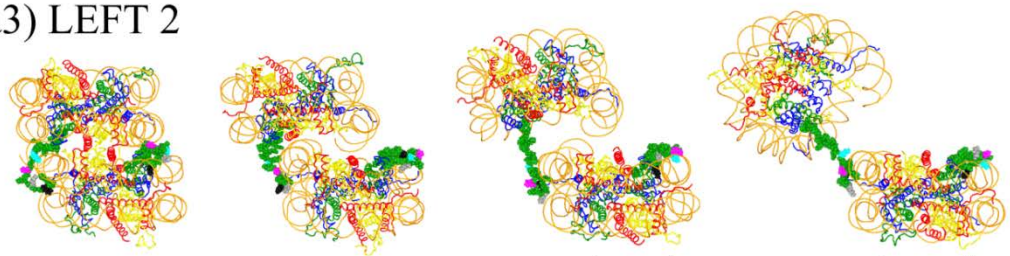

d = 58 Å (13.1 / 12.8 Å)

d = 74 Å (24.8 / 29.4 Å)

d = 90 Å (37.6 / 50.1 Å)

d = 117 Å (52.6 / 116.1 Å)

(a4) LEFT 3

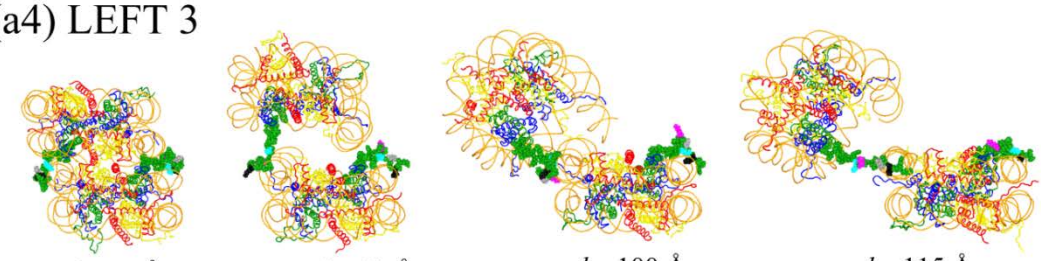

d = 58 Å (13.6 / 11.0 Å)

d = 81 Å (34.1 / 26.7 Å)

d = 100 Å (42.6 / 82.7 Å)

d = 115 Å (57.8 / 105.7 Å)

(b1) RIGHT 1

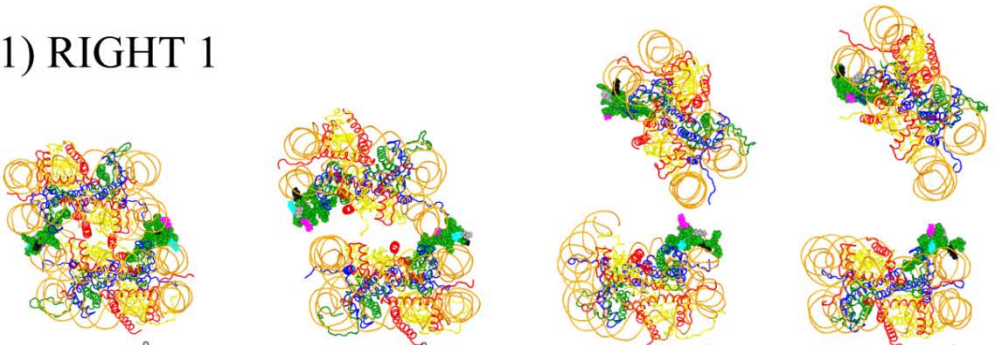

d = 58 Å (11.5 / 9.6 Å)

d = 70 Å (28.5 / 12.1 Å)

d = 108 Å (99. 2 / 35.3 Å)

d = 125 Å (105.2 / 60.5 Å)

(b2) RIGHT 1 (without H4 tails)

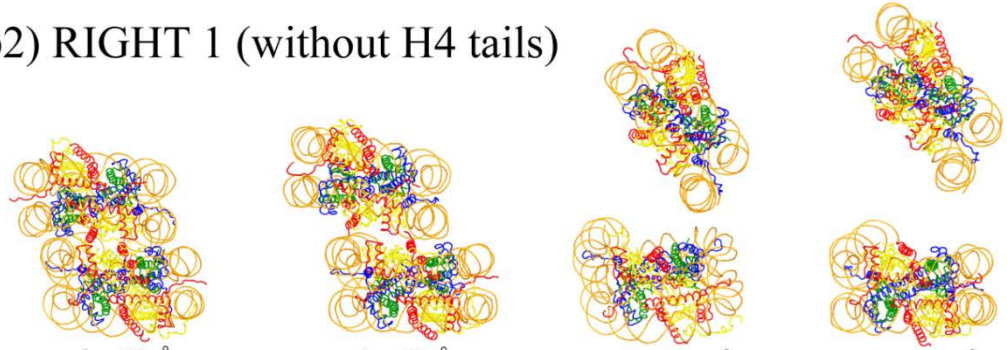

d = 58 Å (11.1 / 11.1 Å)

d = 70 Å (28.7 / 22.2 Å)

d = 108 Å (102.6 / 38.7 Å)

d = 125 Å (104.0 / 65.8 Å)

(b3) RIGHT 2

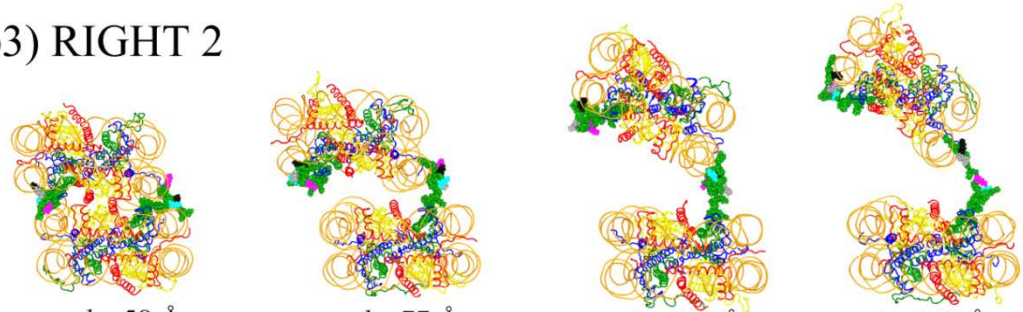

d = 58 Å (13.3 / 10.8 Å)

d = 77 Å (31.4 / 22.9 Å)

d = 100 Å (69.3 / 38.4 Å)

d = 119 Å (99.0 / 63.4 Å)

(b4) RIGHT 3

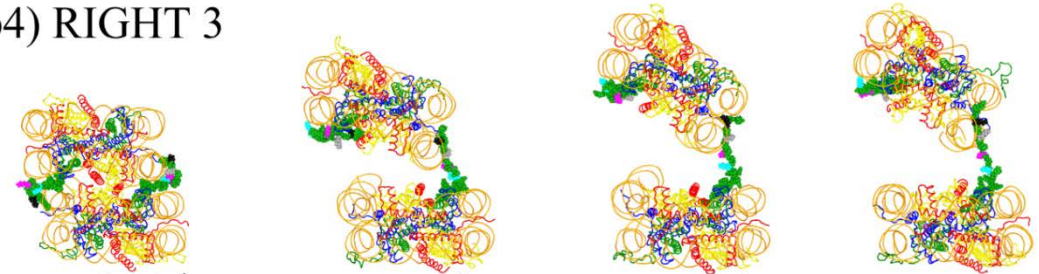

d = 58 Å (11.7 / 10.2 Å)

d = 89 Å (52.0 / 36.6 Å)

d = 100 Å (71.1 / 35.8 Å)

d = 107 Å (85.6 / 40.3 Å)

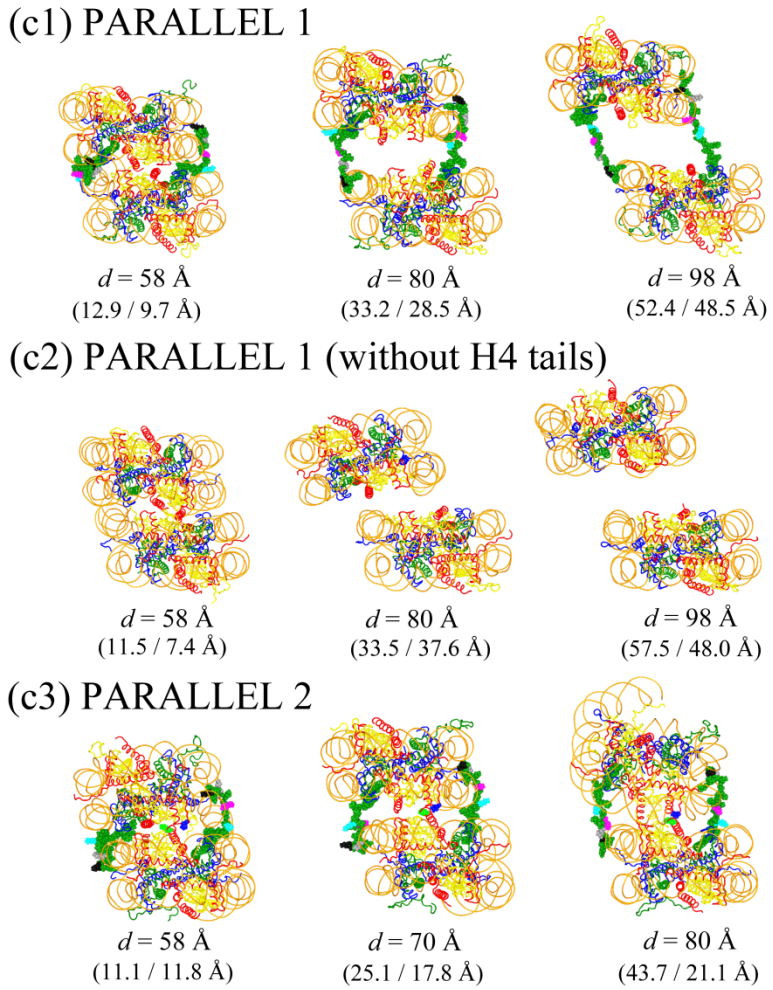

Fig. S8 The snap shots of the NCP-NCP conformations whose $d(\mathrm{DNAs})_{2/1}$ are close to their averages at each d are shown. The value in the bracket after $d(\mathrm{DNAs})_{2/1}$ is the averaged value of $d(\mathrm{DNAs})_{2/1}$ at d. Lys5, Lys8, Lys12 and Lys16 in the H4 $\mathrm{tails}_{2/1}$ are shown in CPK models in black, grey, magenta and cyan, respectively. The side view for each conformation is slightly different from each other for the sake of visual clarity. In PARALLEL 2, Lys177 in $\mathrm{H2B_1}$ and Pro47 in $\mathrm{H2B_2}$ are shown in CPK models in thin green and blue, respectively. It should be noted that $d(\mathrm{DNAs})_{2/1}$ are not necessarily discernable in this figure; for example, although $d(\mathrm{DNAs})_2$ in PARALLEL 1 without the H4 tails, 57.5Å is larger than that with the H4 tails, 52.4Å, the former looks shorter because the $\mathrm{NCP_2}$ has been slid forward and this movement cannot be shown in this figure.

The value of $d(\mathrm{DNAs})_{2/1}$ in the figure and average value of $d(\mathrm{DNAs})_{2/1}$ at each d are shown as follows (the average value is shown in brackets):

(a1) LEFT 1 (i) d = 58 Å, $d(\mathrm{DNAs})_{2/1}$ = 12.5 / 10.8 Å (12.4 / 10.5 Å) ii) d = 75 Å,

d(DNAs)$_{2/1}$ = 19.5 / 32.0 Å, (19.8 / 32.1 Å) (iii) d = 90 Å, d(DNAs)$_{2/1}$ = 22.4 / 71.5 Å (22.4 / 71.4 Å) and (iv) d = 111 Å, d(DNAs)$_{2/1}$ = 26.4 / 136.6 Å (135.5 / 26.8 Å)
(a2) LEFT 1 without the H4 tails (i) d = 58 Å, d(DNAs)$_{2/1}$ = 9.5 / 7.3 Å (9.4 / 7.3 Å) ii) d = 75 Å, d(DNAs)$_{2/1}$ = 23.0 / 31.6 Å (23.0 / 31.8 Å), (iii) d = 90 Å, d(DNAs)$_{2/1}$ = 28.8 / 68.5 Å (29.6 / 68.6 Å) and (iv) d = 111 Å, d(DNAs)$_{2/1}$ = 34.0 / 129.6 Å (34.5 / 128.9 Å)
(a3) LEFT 2 (i) d = 58 Å, d(DNAs)$_{2/1}$ = 13.1 / 12.8 Å (13.0 / 12.8 Å) ii) d = 74 Å, d(DNAs)$_{2/1}$ = 24.8 / 29.4 Å (24.3 / 29.1 Å), (iii) d = 90 Å, d(DNAs)$_{2/1}$ = 37.6 / 50.1 Å (37.9 / 50.8 Å) and (iv) d = 117 Å, d(DNAs)$_{2/1}$ = 52.6 / 116.1 Å (52.9 / 115.7 Å)
(a4) LEFT 3 (i) d = 58 Å, d(DNAs)$_{2/1}$ = 13.6 / 11.0 Å (13.5 / 11.3 Å) ii) d = 81 Å, d(DNAs)$_{2/1}$ = 34.1 / 26.7 Å (35.0 / 27.2 Å), (iii) d = 100 Å, d(DNAs)$_{2/1}$ = 42.6 / 82.7 Å (42.3 / 82.8 Å) and (iv) d = 115 Å, d(DNAs)$_{2/1}$ = 57.8 / 105.7 Å (57.2 / 105.5 Å)

(b1) RIGHT 1 (i) d = 58 Å, d(DNAs)$_{2/1}$ = 11.5 / 9.6 Å (11.3 / 9.5 Å) ii) d = 70 Å, d(DNAs)$_{2/1}$ = 28.5 / 12.1 Å (28.7 / 12.4 Å), (iii) d = 108 Å, d(DNAs)$_{2/1}$ = 99.2 / 35.3 Å (99.2 / 36.8 Å) and (iv) d = 125 Å, d(DNAs)$_{2/1}$ = 105.2 / 60.5 Å (105.8 / 60.7 Å)
(b2) RIGHT 1 without the H4 tails (i) d = 58 Å, d(DNAs)$_{2/1}$ = 11.1 / 11.1 Å (11.1 / 11.4 Å) ii) d = 70 Å, d(DNAs)$_{2/1}$ = 28.7 / 22.2 Å (28.5 / 22.1 Å), (iii) d = 108 Å, d(DNAs)$_{2/1}$ = 102.6 / 38.7 Å (101.7 / 38.4 Å) and (iv) d = 125 Å, d(DNAs)$_{2/1}$ = 104.0 / 65.8 Å (103.8 / 65.0 Å)
(b3) RIGHT 2 (i) d = 58 Å, d(DNAs)$_{2/1}$ = 13.3 / 10.8 Å (13.1 / 10.8 Å) ii) d = 77 Å, d(DNAs)$_{2/1}$ = 31.4 / 22.9 Å (32.1 / 22.4 Å), (iii) d = 100 Å, d(DNAs)$_{2/1}$ = 69.3 / 38.4 Å (69.6 / 39.5 Å) and (iv) d = 119 Å, d(DNAs)$_{2/1}$ = 99.0 / 63.4 Å (99.6 / 63.1 Å)
(b4) RIGHT 3 (i) d = 58 Å, d(DNAs)$_{2/1}$ = 11.7 / 10.2 Å (11.7 / 10.0 Å) ii) d = 89 Å, d(DNAs)$_{2/1}$ = 52.0 / 36.6 Å, (52.9 / 36.4 Å) (iii) d = 100 Å, d(DNAs)$_{2/1}$ = 71.1 / 35.8 Å (71.0 / 36.6 Å) and (iv) d = 107 Å, d(DNAs)$_{2/1}$ = 85.61 / 40.3 Å (85.4 / 40.7 Å)

(c1) PARALLEL 1 (i) d = 58 Å, d(DNAs)$_{2/1}$ = 12.9 / 9.7 Å (12.8 / 9.7 Å) ii) d = 80 Å, d(DNAs)$_{2/1}$ = 33.2 / 28.5 Å (33.3 / 28.4 Å) iii) d = 98 Å, d(DNAs)$_{2/1}$ = 52.4 / 48.5 Å (52.4 / 48.5 Å)
(c2) PARALLEL 1 without the H4 tails (i) d = 58 Å, d(DNAs)$_{2/1}$ = 11.5 / 7.4 Å (11.6 / 7.7 Å) ii) d = 80 Å, d(DNAs)$_{2/1}$ = 33.5 / 37.6 (33.5 / 37.6 Å) iii) d = 98 Å, d(DNAs)$_{2/1}$ = 57.5 / 48.0 Å (57.5 / 48.2 Å)
(c3) PARELLEL 2 (i) d = 58 Å, d(DNAs)$_{2/1}$ = 11.1 / 11.8 Å (11.6 / 11.4 Å) ii) d = 70 Å, d(DNAs)$_{2/1}$ = 25.1 / 17.8 Å (25.3 / 17.2 Å) and (iii) d = 80 Å, d(DNAs)$_{2/1}$ = 43.7 / 21.1 Å (43.5 / 21.9 Å)

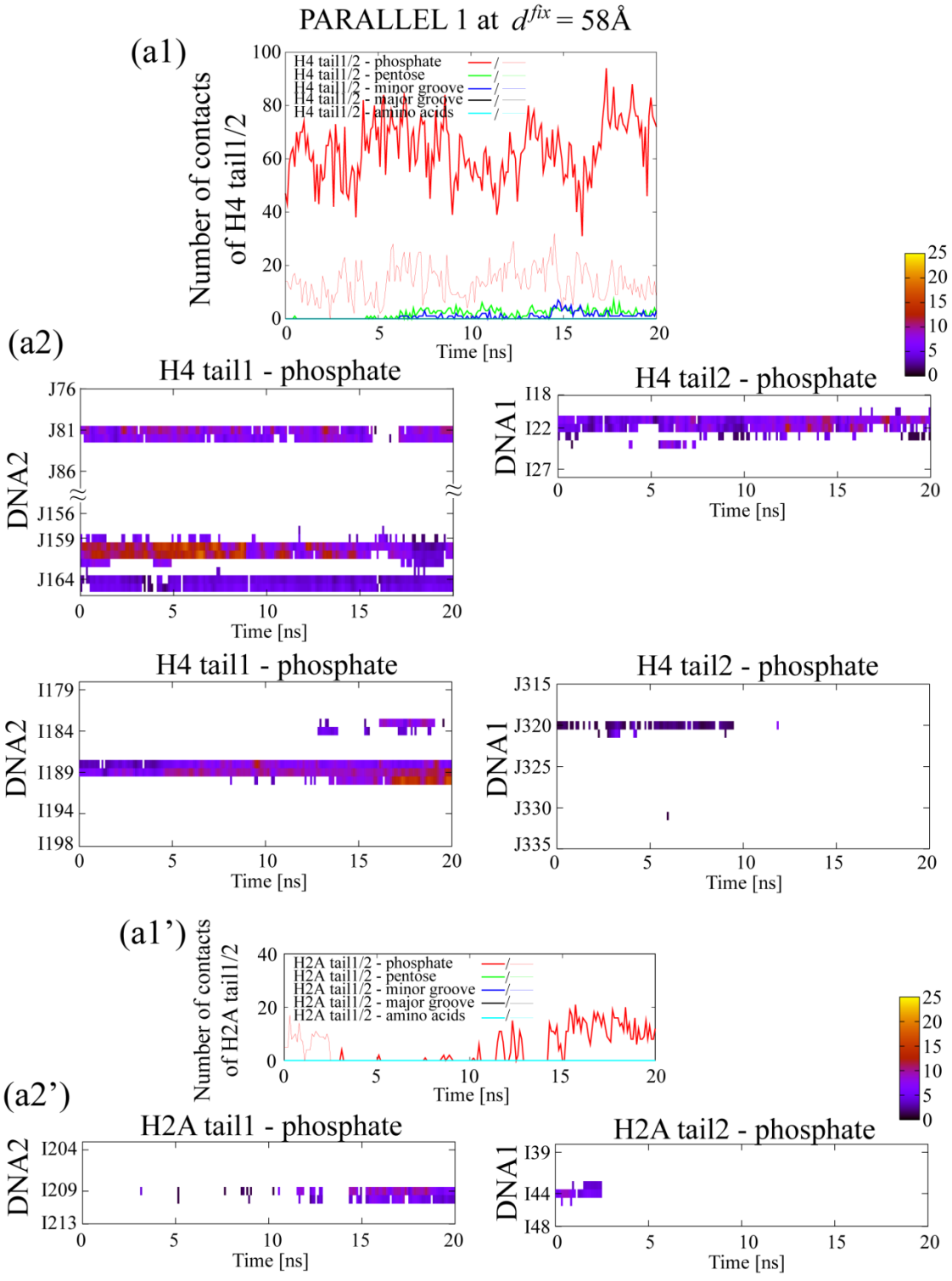
PARALLEL 1 at d^{fix} = 58Å
(a1)
Number of contacts of H4 tail1/2
H4 tail1/2 - phosphate
H4 tail1/2 - pentose
H4 tail1/2 - minor groove
H4 tail1/2 - major groove
H4 tail1/2 - amino acids
Time [ns]
(a2)
H4 tail1 - phosphate
H4 tail2 - phosphate
DNA2
DNA1
Time [ns]
(a1')
Number of contacts of H2A tail1/2
H2A tail1/2 - phosphate
H2A tail1/2 - pentose
H2A tail1/2 - minor groove
H2A tail1/2 - major groove
H2A tail1/2 - amino acids
(a2')
H2A tail1 - phosphate
H2A tail2 - phosphate

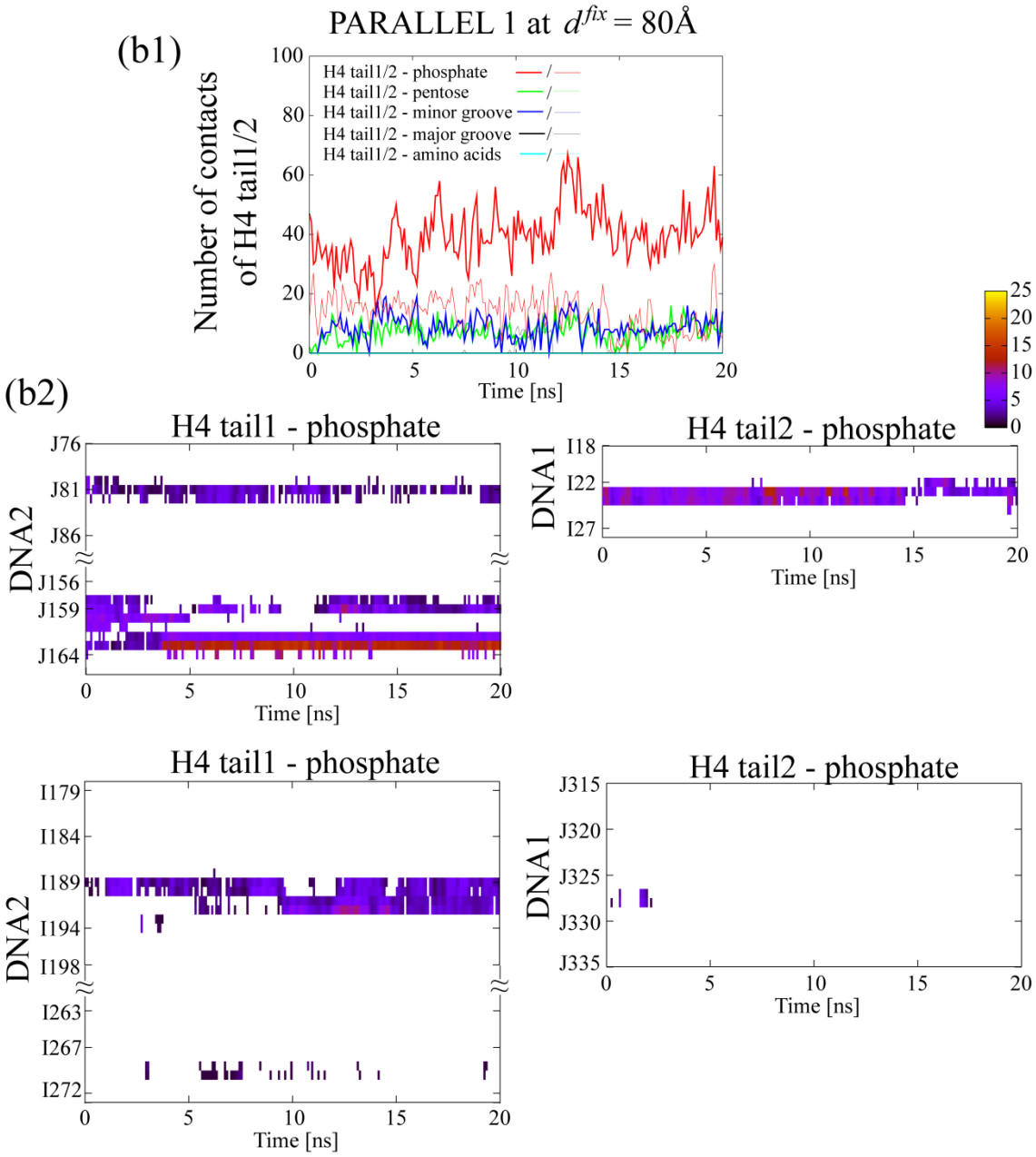
(b1)
PARALLEL 1 at d^{fix} = 80Å
Number of contacts of H4 tail1/2
H4 tail1/2 - phosphate
H4 tail1/2 - pentose
H4 tail1/2 - minor groove
H4 tail1/2 - major groove
H4 tail1/2 - amino acids
Time [ns]
(b2)
H4 tail1 - phosphate
H4 tail2 - phosphate
DNA2
DNA1
Time [ns]

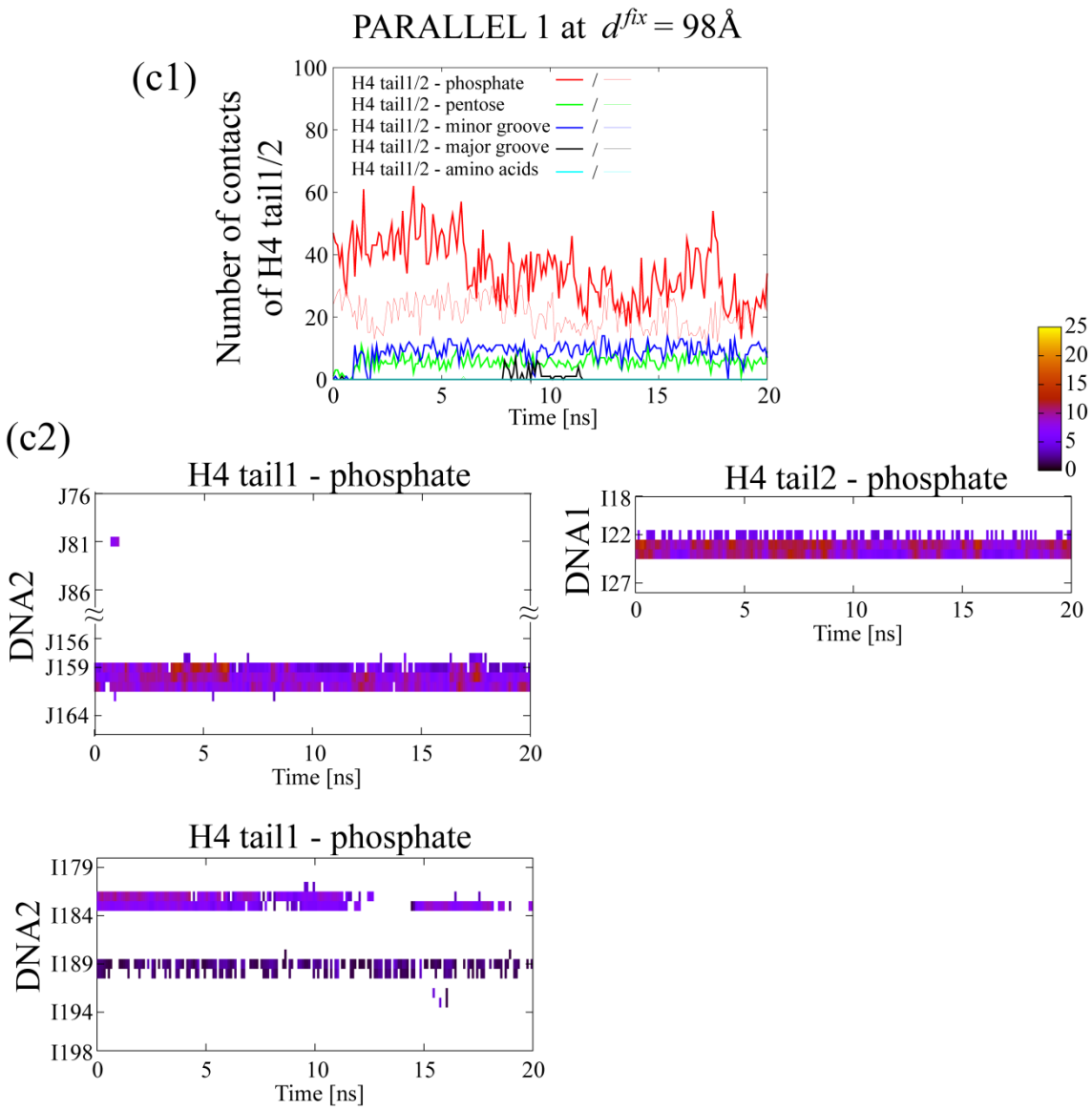
PARALLEL 1 at $d^{fix} = 98$Å
(c1)
Number of contacts of H4 tail1/2
H4 tail1/2 - phosphate
H4 tail1/2 - pentose
H4 tail1/2 - minor groove
H4 tail1/2 - major groove
H4 tail1/2 - amino acids
Time [ns]
(c2)
H4 tail1 - phosphate
DNA2
J76
J81
J86
J156
J159
J164
Time [ns]
H4 tail2 - phosphate
DNA1
I18
I22
I27
Time [ns]
H4 tail1 - phosphate
DNA2
I179
I184
I189
I194
I198
Time [ns]

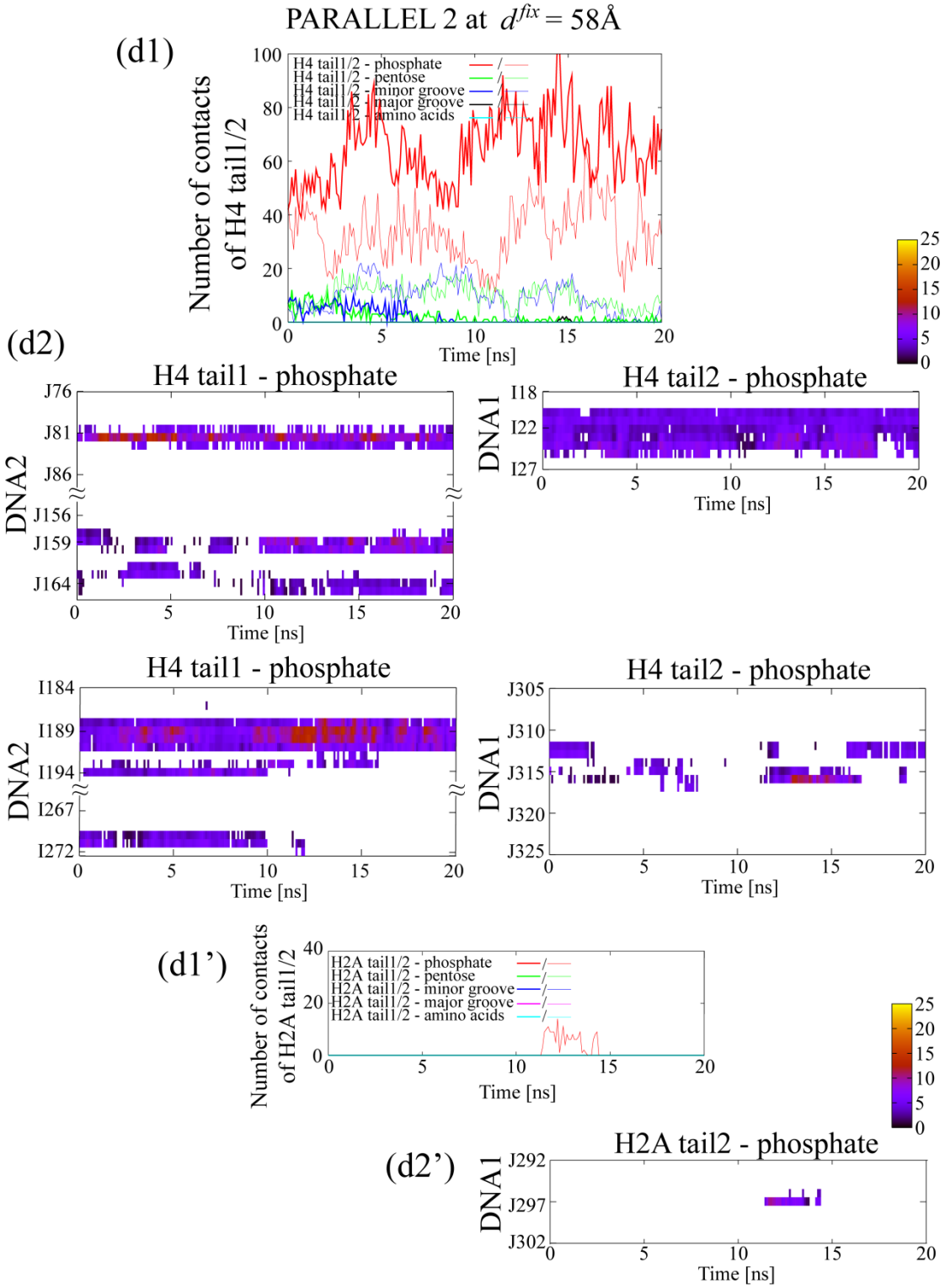
PARALLEL 2 at d^{fix} = 58Å
(d1)
Number of contacts of H4 tail1/2
H4 tail1/2 - phosphate
H4 tail1/2 - pentose
H4 tail1/2 - minor groove
H4 tail1/2 - major groove
H4 tail1/2 - amino acids
Time [ns]
(d2)
H4 tail1 - phosphate
H4 tail2 - phosphate
DNA2
DNA1
J76
J81
J86
J156
J159
J164
I18
I22
I27
I184
I189
I194
I267
I272
J305
J310
J315
J320
J325
Time [ns]
(d1')
Number of contacts of H2A tail1/2
H2A tail1/2 - phosphate
H2A tail1/2 - pentose
H2A tail1/2 - minor groove
H2A tail1/2 - major groove
H2A tail1/2 - amino acids
Time [ns]
(d2')
H2A tail2 - phosphate
DNA1
J292
J297
J302
Time [ns]

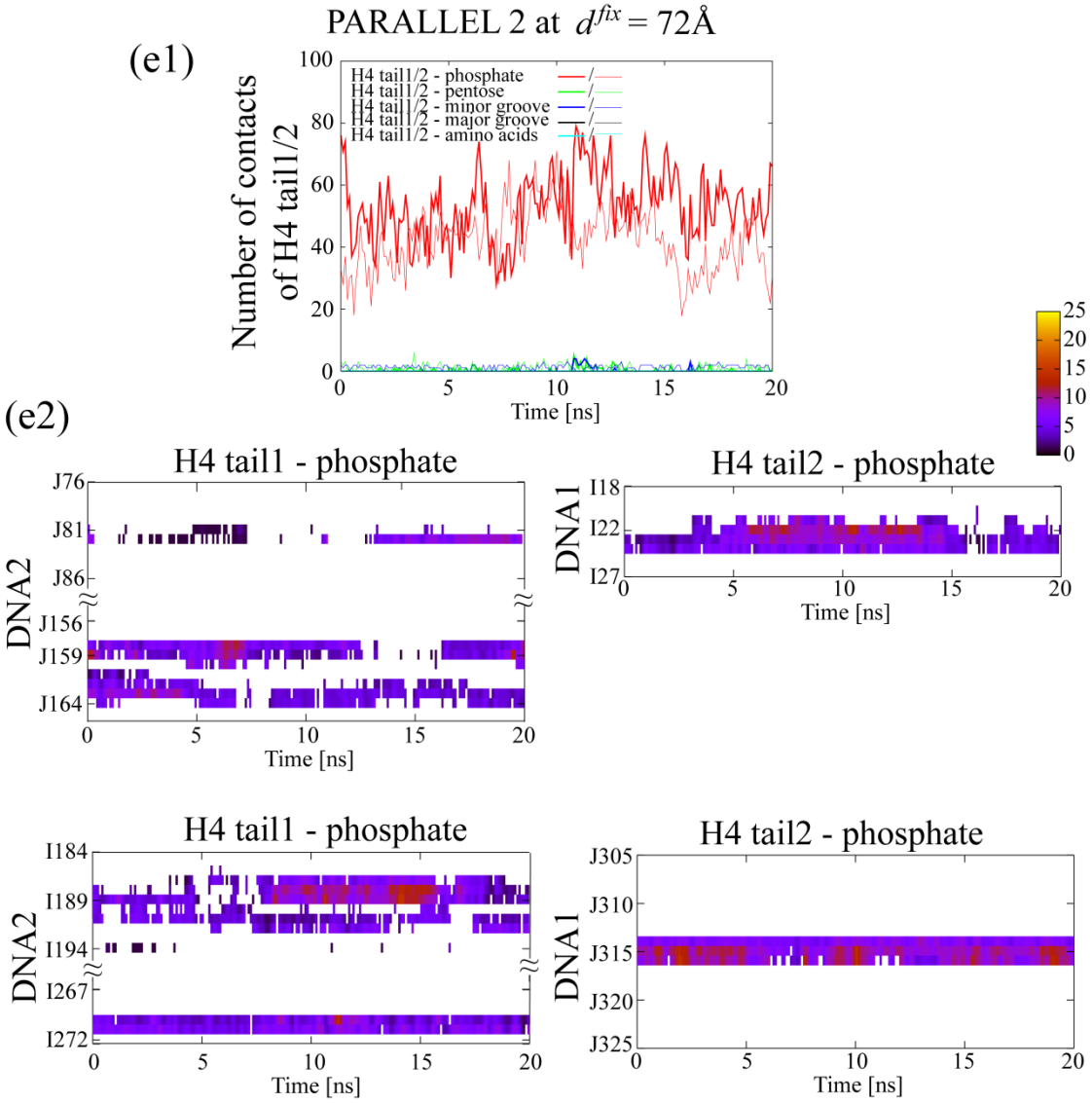
PARALLEL 2 at d^{fix} = 72Å
(e1)
Number of contacts of H4 tail1/2
H4 tail1/2 - phosphate
H4 tail1/2 - pentose
H4 tail1/2 - minor groove
H4 tail1/2 - major groove
H4 tail1/2 - amino acids
Time [ns]
(e2)
H4 tail1 - phosphate
H4 tail2 - phosphate
DNA2
DNA1
J76
J81
J86
J156
J159
J164
I18
I22
I27
H4 tail1 - phosphate
H4 tail2 - phosphate
I184
I189
I194
I267
I272
J305
J310
J315
J320
J325
Time [ns]

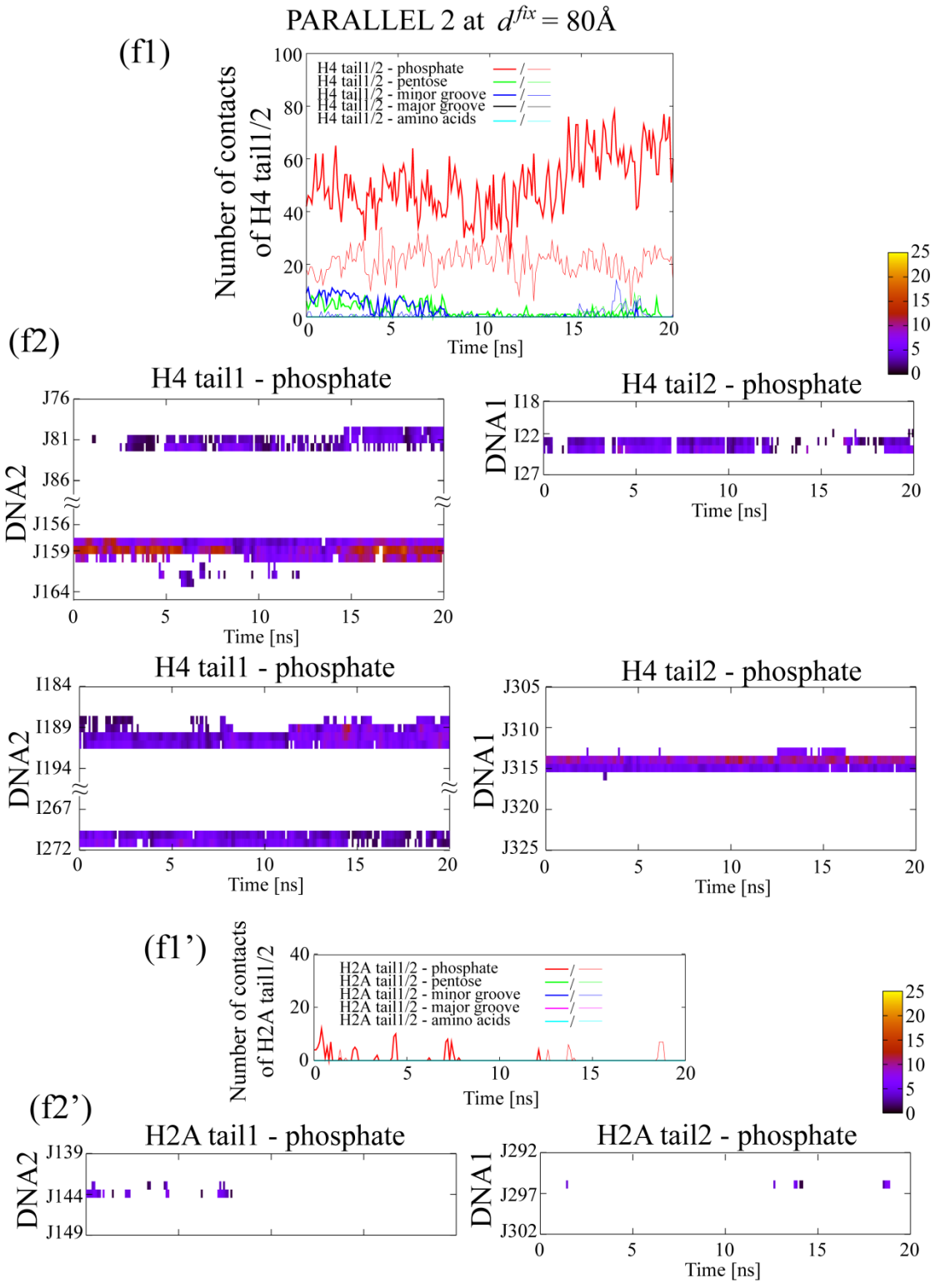

Fig. S9 The number of contacts within 3.5 Å between the (H4 and H2A) tails and the neighboring NCP for the last 20 ns of the umbrella sampling simulation in PARALLEL 1 at (a) d^{fix} = 58 (b) 80 and (c) 98 Å, and PARALLEL 2 at (d) d^{fix} = 58

(e) 72 and (f) 80 Å is shown. To observe the screening effect of the NCP-NCP repulsion, the side-chain atoms of positively charged amino acids, Lys and Arg (Arg3, Lys5, Lys8, Lys12, Lys16, Arg17, Arg19, Lys20, Arg23 in the H4 $tail_{1/2}$, and Arg3, Lys5, Lys9, Arg11, Lys13, Lys15 in H2A $tail_{1/2}$), the atoms of phosphate group (O1P, O2P, O3', O5'), pentose (O4' of the pentose), minor groove (N3 of adenine and guanine, O2 of thymine and cytosine) and major groove (O6 and N7 of guanine, N7 of adenine, O4 of thymine) in the DNA, the side-chain atoms of negatively charged amino acids (Asp and Glu) in the histone octamer were selected for the analysis. The data was analyzed from the trajectory of every 100 ps for the last 20 ns of the umbrella sampling.

The vertical axes in (a1-f1) show the contact numbers of H4 $tail_{1/2}$ and the vertical axes in (a1'), (d1') and (f1') show the contact numbers of the H2A $tail_{1/2}$. The vertical axes in (a2-f2) show the nucleotides in which atoms of the phosphate group interacted with the H4 $tails_{1/2}$, and the vertical axes in (a2'), (d2') and (f2') show the nucleotides in which atoms of the phosphate group interacted with the H2A $tail_{1/2}$. Contact between H2A $tail_{1/2}$ and $DNA_{2/1}$ was not observed at d^{fix} = 80 and 98 Å in PARALLEL 1 and at d^{fix} = 72 Å in PARALLEL 2.

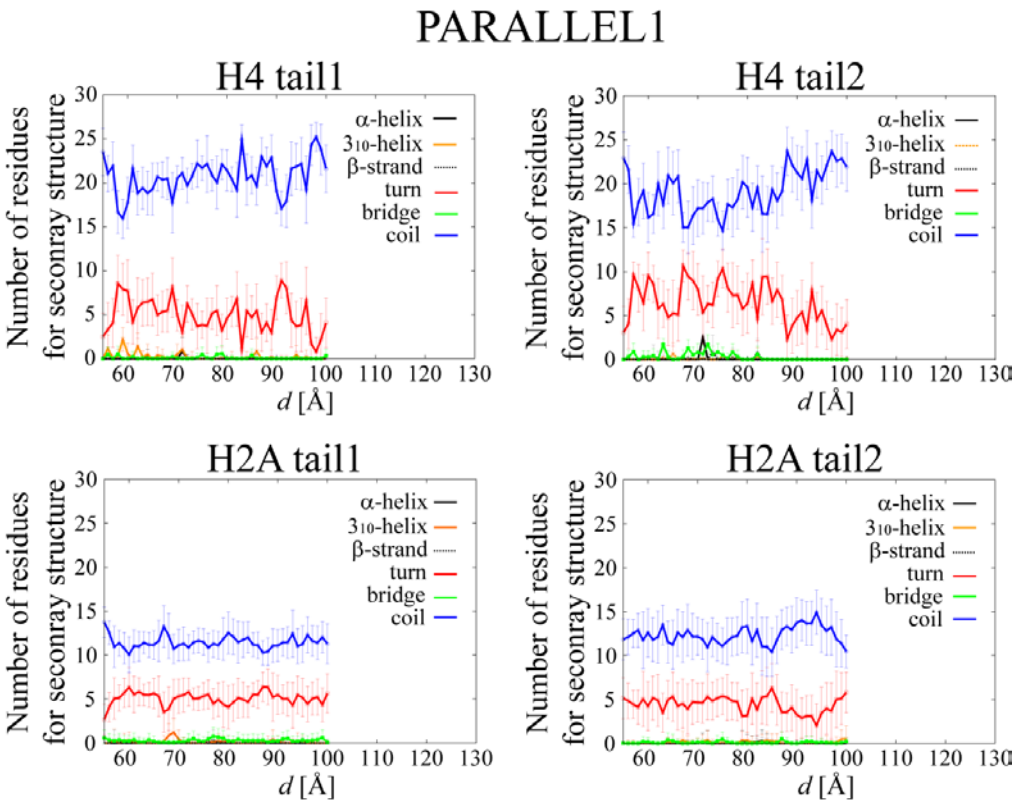

Fig. S10　The average numbers of residues forming α-helix, 3_{10}-helix, β-strand, turn and random coil in the 26 residues in the H4 $tail_{1/2}$ and 17 residues in the H2A $tails_{1/2}$ in PARALLEL 1 are shown against *d*, respectively.　The number of residues forming secondary structures was analyzed using software called STRIDE (19).

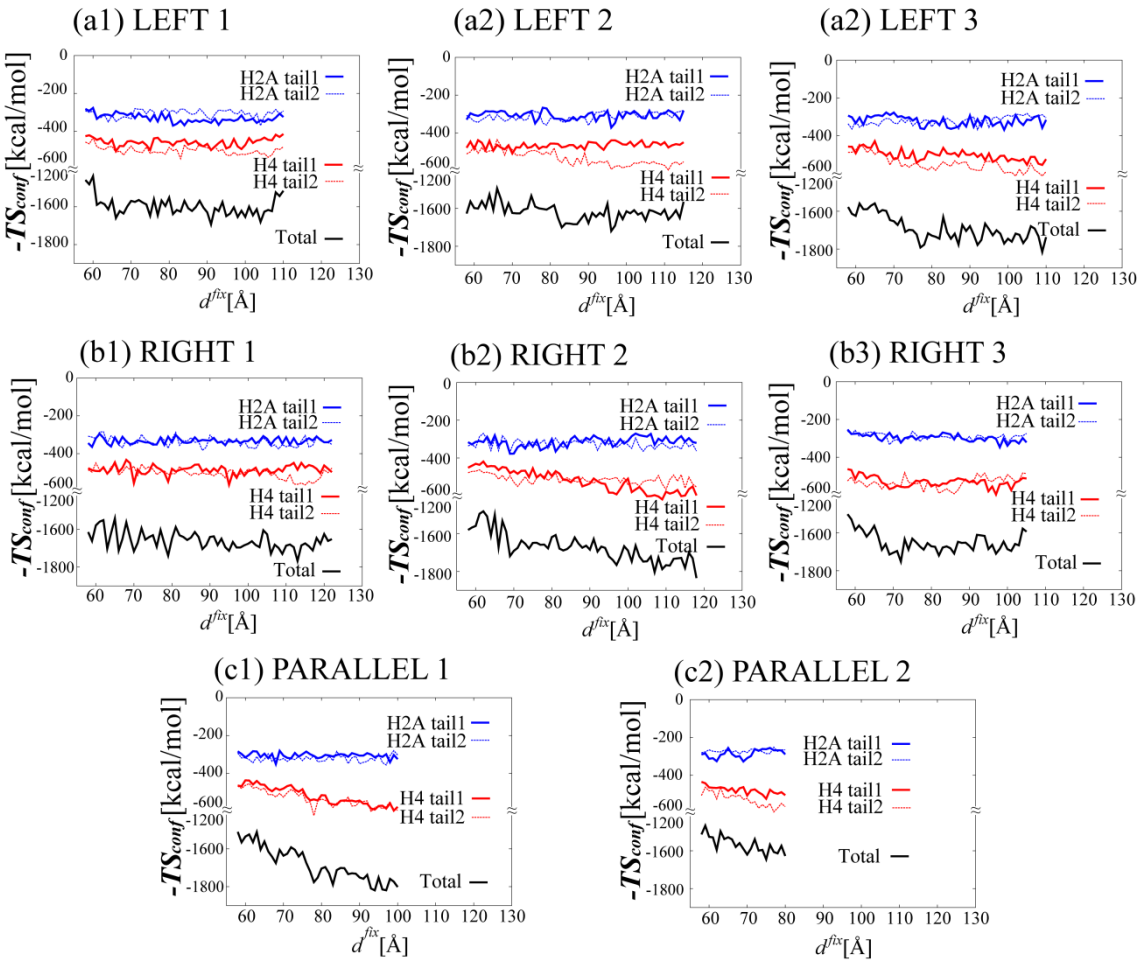

Fig. S11 The conformational entropies of the H4 and H2A tails are shown against d^{fix} in blue and red, respectively. Their total is shown in black.

$-TS_{conf}$ decreased as d^{fix} increased in general. The decrease is clear in LEFT 3, RIGHT 2 and PARALLELs 1-2. However, there were places where $-TS_{conf}$ increased after d^{fix} = ~ 107 Å in RIGHT 1 and after d^{fix} = ~ 90 Å in RIGHT 3. In RIGHT 1, $-TS_{conf}$ of the H4 $tail_1$ increased probably because the H4 $tail_1$ detached from the DNA_2 in the umbrella sampling simulation at d^{fix} = ~ 107 Å during which many conformations were sampled at d = ~ 108 Å, and the detached H4 $tail_1$ stayed on the DNA of its own NCP after d = 108 Å (Fig. S8(b1)). In RIGHT 3, $-TS_{conf}$ of the H4 $tail_2$ increased probably because the H4 $tail_2$ detached from the DNA_1 in the umbrella sampling simulation at d^{fix} = ~ 90 Å during which many conformations were sampled at d = ~ 89 Å, and the detached H4 $tail_2$ stayed on the DNA of its own NCP after d = 89 Å (Fig. S8(b4)).

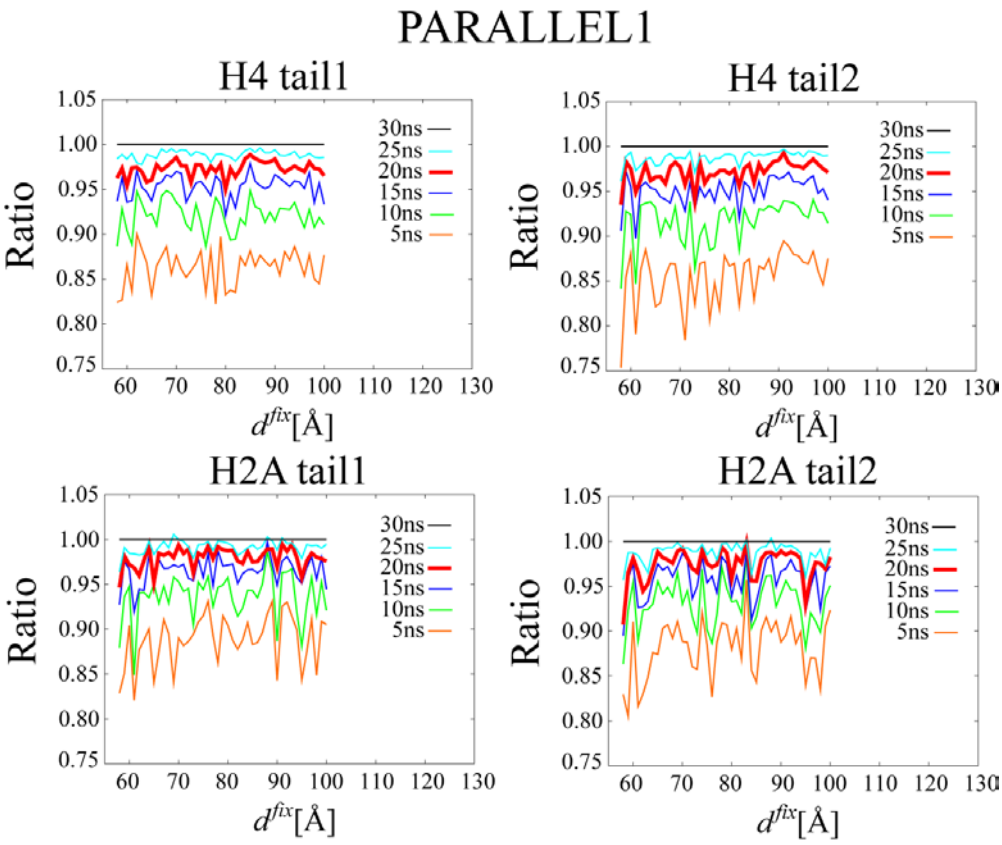

Fig. S12 The convergence for the conformational entropies of the H4 and H2A tails in PARALLEL 1. The ratios of the conformational entropies of the H4 $tail_{1/2}$ and H2A $tail_{1/2}$ for 5 ns (from 10 to 15 ns), 10 ns (from 10 to 20 ns), 15 ns (from 10 to 25 ns), 20 ns (from 10 to 30 ns), 25 ns (from 5 to 30 ns) and 30 ns (from 0 to 30 ns) are shown against those for 30 ns in the umbrella sampling simulations.

Convergence of the conformational entropy of the H2B tails was better than that of the H4 tails probably because the H2B tails are shorter than the H4 tails and the dynamics of the H2B tails were more localized.

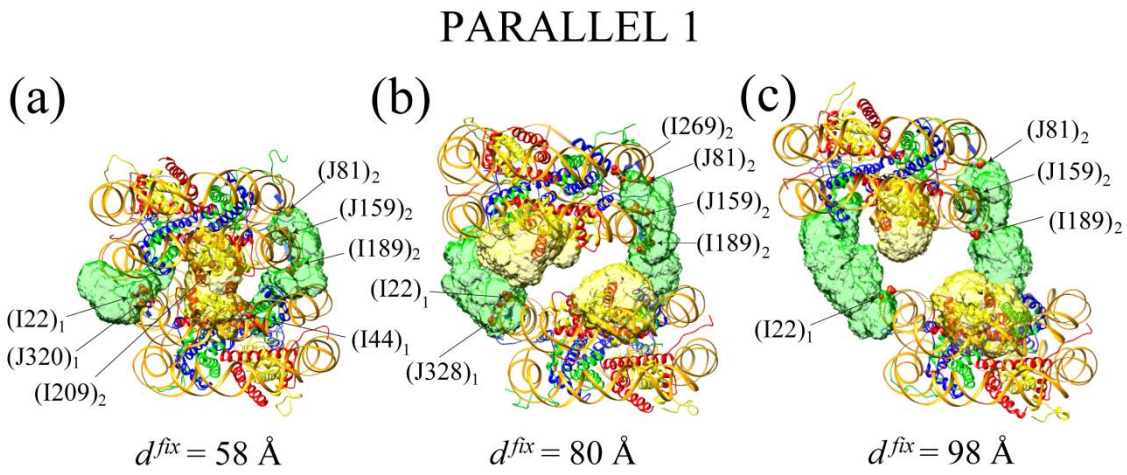

Fig. S13 The spatial distribution of all the atoms in the H4 (in green) and H2A tails (in yellow) in PARALELL 1 at (a) d^{fix} = 58 Å, (b) 80 Å and (c) 98 Å for the last 20 ns of the umbrella sampling simulation. The umbrella sampling simulation at d^{fix} sampled the conformation of the NCPs at d = ~ 58, 80 and 98 Å in Fig. S8(c1). The volumes covered by the atoms in the H4 $tails_{1/2}$ and H2A $tails_{1/2}$ were 14453 / 17517 $Å^3$ and 9637 / 10177 $Å^3$ at d^{fix} = 58 Å, 23140 / 28426 $Å^3$ and 15953 / 20514 $Å^3$ at d^{fix} = 80 Å, 30374 / 31035 $Å^3$ and 23896 / 14977 $Å^3$ at d^{fix} = 98 Å, respectively. To calculate the spatial distribution, the sampled coordinates were located so that the rigid parts of the two NCPs (Gly33−Ala135 of H3, Asn25−Gly102 of H4, Lys15−Thr120 of H2A, and Pro50−Lys125 of H2B histones which were also used to calculate the reaction coordinate) best-fit to the reference coordinate. The initial structure in the *i*-th window of the umbrella sampling simulation was used as the reference coordinate for the best-fit at d_i^{fix}. Some nucleotides in $DNA_{1/2}$ which interacted with Lys and Arg in the H4 and H2A tails are shown in CPK model. The figure was created using Chimera software (20).

For reference, the conformational entropies of the H4 $tails_{1/2}$ and H2A $tails_{1/2}$ were −465.0 / −467.9 kcal/mol and −284.2 / −293.1 kcal/mol at d^{fix} = 58 Å, −516.0 / −536.0 kcal/mol and −315.8 / −336.4 kcal/mol at d^{fix} = 80 Å and −559.1 / −551.3 kcal/mol and −341.8 / −306.8 kcal/mol at d^{fix} = 98 Å, respectively (Fig. S11).

SUPPORTING REFERENCES

1. Ishida, H. and S. Hayward. 2008. Path of Nascent Polypeptide in Exit Tunnel Revealed by Molecular Dynamics Simulation of Ribosome. Biophysical J. 95:5962-5973.
2. Ishida, H. 2010. Branch Migration of Holliday Junction in RuvA Tetramer Complex Studied by Umbrella Sampling Simulation Using a Path-Search Algorithm. J. Comput. Chem. 31:2317-2329.
3. Ishida, H. and A. Matsumoto. 2014. Free-Energy Landscape of Reverse tRNA Translocation through the Ribosome Analyzed by Electron Microscopy Density Maps and Molecular Dynamics Simulations. PLOS ONE 9:e101951.
4. Ishida, H. 2014. Essential function of the N-termini tails of the proteasome for the gating mechanism revealed by molecular dynamics simulations. Proteins 82:1985-1999.
5. Ishida, H. and A. Matsumoto. 2016. Mechanism for verification of mismatched and homoduplex DNAs by nucleotides-bound MutS analyzed by molecular dynamics simulations. Proteins.
6. Hornak, V., R. Abel, A. Okur, B. Strockbine, A. Roitberg, and C. Simmerling. 2006. Comparison of multiple amber force fields and development of improved protein backbone parameters. Proteins 65:712-725.
7. Pérez, A., I. Marchán, D. Svozil, J. Sponer, T. E. Cheatham, C. A. Laughton, and M. Orozco. 2007. Refinement of the AMBER Force Field for Nucleic Acids: Improving the Description of α/γ Conformers. Biophysical J. 92:3817-3829.
8. Joung, I. S. and T. E. Cheatham. 2008. Determination of alkali and halide monovalent ion parameters for use in explicitly solvated biomolecular simulations. J. Phys. Chem. B 112:9020-9041.
9. Jorgensen, W. L., J. Chandrasekhar, J. D. Madura, R. W. Impey, and M. L. Klein. 1983. Comparison of simple potential functions for simulating liquid water. J. Chem. Phys. 79:926-935.
10. Hockney, R. W. and J. W. Eastwood, editors. 1988. Computer simulation using particles: Adam Hilger, New York.
11. Deserno, M. and C. Holm. 1998. How to mesh up Ewald sums. I. A theoretical and numerical comparison of various particle mesh routines. J. Chem. Phys. 109:7678-7693.
12. Ryckaert, J., G. Cicotti, and H. J. C. Berendsen. 1977. Numerical integraton of the Cartesian equations of motion of a system with constraints: molecular

dynamics of *n*-alkanes. J. Comput. Phys. 23:327-341.

13. van Gunsteren, W. F. and H. J. C. Berendsen. 1977. Algorithms for macromolecular dynamics and constraint dynamics. Mol. Phys. 34:1311-1327.
14. Babin, V., C. Roland, and C. Sagui. 2008. Adaptively biased molecular dynamics of free energy calculations. J. Chem. Phys. 128:134101.
15. Raiteri, P., A. Laio, F. L. Gervasio, C. Micheletti, and M. Parrinello. 2006. Efficient Reconstruction of Complex Free Energy Landscapes by Multiple Walkers Metadynamics. J. Phys. Chem. B. 110:3533-3539.
16. Kumar, S., D. Bouzida, R. H. Swendsen, P. A. Kollman, and J. M. Rosenberg. 1992. The weighted histogram analysis method for free energy calculations on biomolecules. I. The method. J. Comput. Chem. 13:1011-1021.
17. Schlitter, J. 1993. Estimation of Absolute and Relative Entropies of Macromolecules Using the Covariance Matrix. Chem. Phys. Lett. 215:617-621.
18. Schalch, T., S. Duda, D. F. Sargent, and T. J. Richmond. 2005. X-ray structure of a tetranucleosome and its implications for the chromatin fibre. Nature 436:138-141.
19. Frishman, D. and P. Argos. 1995. Knowledge-Based Protein Secondary Structure Assignment. Proteins 23:566-579.
20. Pettersen, E. F., T. D. Goddard, C. C. Huang, G. S. Couch, D. M. Greenblatt, E. C. Meng, and T. E. Ferrin. 2004. UCSF Chimera—a visualization system for exploratory research and analysis. J. Comput. Chem. 25:1605.